EVALUATION OF LONG TERM DURABILITY IN CONCRETE WITH EXTERNAL PRE-SATURATED CFRP LAMINATE

by

RAMYA ANANDHAN

Presented to the Faculty of the Graduate School of

The University of Texas at Arlington in Partial Fulfillment

of the Requirements

for the Degree of

MASTER OF SCIENCE IN CIVIL ENGINEERING

THE UNIVERSITY OF TEXAS AT

ARLINGTON

AUGUST 2020

Acknowledgements

I would like to express my deep and sincere gratitude to my advisor, Dr. Nur Yazdani, for providing constant support and encouragement, and sharing his immense knowledge throughout this research.

I would like to thank my committee members, Dr. Srinivas Prabakar and Dr. Chao, for agreeing to be part of my research.

I want to express my special thanks to Dr. Kent L Lawrence of the Mechanical and Aerospace Department of The University of Texas at Arlington. Dr. Lawrence was always available when I needed help with my design.

I would also like to extend my gratitude to Dr Eyosias, whose guidance helped me during the research and writing of this thesis.

And I would like to take this opportunity to express my gratitude to my group members whose support, guidance and assistance made the completion of this thesis possible.

Last but not least, I owe my greatest gratitude to my husband, Sathish, my daughter, Sara, and my family and friends for their continuous support and patience during my graduate studies.

Abstract

EXPERIMENTAL AND NUMERICAL STUDY ON CHLORIDE INGRESS AND WATER PERMEABILITY OF PRESATURATED CARBON FIBER REINFORCED POLYMER WRAPPED CONCRETE

Ramya Anandhan, MS

The University of Texas at Arlington, 2020

Supervising Professor: Nur Yazdani

Many studies have investigated the use of carbon fiber reinforced polymer (CFRP) wraps to strengthen structural members, but there is limited literature on the application of presaturated CFRP wraps on reinforced concrete members. The main objective of this research is to study the long-term effectiveness of presaturated CFRP wraps in preventing corrosion of reinforced concrete specimens in severe environments. This paper presents numerical and experimental studies that were conducted to determine whether CFRP presaturated wraps provide a barrier against the ingress of chloride and permeability of water into concrete and thereby decelerate the corrosion process. The results show that the presaturated CFRP laminates, wrapped on high strength and normal strength concrete, provide a stronger barrier against chloride ingress and water permeability than the regular CFRP and control specimens without CFRP. A finite element model was validated with the experimental results, and an extensive parametric study on a typical Texas Department of Transportation (TxDOT) bridge column was conducted to identify the deterioration level of a CFRP-wrapped column in coastal environments. The results suggested that both regular CFRP and presaturated CFRP-wrapped concrete columns reduce the clear cover and can be used to assess the long-term durability of CFRP-wrapped concrete structures.

Table of Contents

List of Figures

List of Tables

Chapter 1 Introduction

1.1 Background

Reinforced concrete structures often are exposed to an aggressive environment that causes a major durability issue that leads to corrosion of the steel reinforcement. The corrosion of the rebars not only affects the durability of the concrete, but also lowers the strength and service life of reinforced concrete structures. The American Society of Civil Engineers Infrastructure Report graded the nation's infrastructure as D+, and almost four in ten bridges, with an average age of 43 years, are deemed structurally deficient. A recent survey shows that the nation needs to spend $123 billion on rehabilitating its bridges (ASCE 2017). Thus, it is crucial to address this need by immediately repairing or strengthening the bridges, since rebuilding is more costly.

The use of carbon fiber reinforced polymers (CFRP) is rapidly gaining acceptance for strengthening concrete structures. CFRP is an externally applied heterogeneous reinforcing material consisting of two parts: a textile-like fabric of carbon strands and a high strength structural epoxy or resin. At the smallest level, the diameter of a carbon fiber filament is merely 7 to 10 micrometers. These filaments are used to form a single carbon fiber strand, and the strands are woven together with a glass or nylon transverse thread to produce a fabric-like sheet (Kobayashi, Kanakubo, & Jinno, 2004). The carbon fiber sheets are then impregnated with a structural epoxy or resin, and the individual fibers act as a unit, as shown in Figure 1-1. Figure 1-2 provides a magnified image of FRP from a scanning electron microscope.

Figure 1-1 Schematic diagram of a CFRP sheet (Yang, 2007)

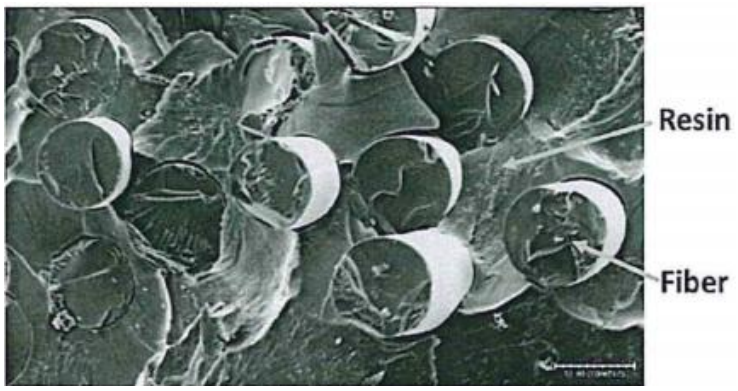

Figure 1-2 Scanning electron microscope image of CFRP (Yungon Kim, 2012)

CFRP materials have many positive qualities that make them attractive to engineers for strengthening. These include mechanical strength and stiffness; corrosion resistance; light weight; easy handling; and their ability to be applied in long strips, eliminating many lap splices (Triantafillou, 1998). Carbon fibers are not affected by harsh conditions such as exposure to high humidity, acids, bases, or other solvents, and they can withstand direct contact with concrete (Malvar, Warren, & Inaba, 1995). In terms of mechanical properties, CFRP is classified as an anisotropic material that maintains high strength in the direction of its fibers, and is an elastic material that maintains a linear stress strain relationship up to failure with typical ultimate strain values of 1 to 1.5%. This means that a CFRP system can provide a large amount of strength with a relatively small amount of material.

A drawback of using CFRP as a retrofitting technique is the high cost of the material. While the structural epoxy or resin is relatively inexpensive, carbon fiber fabric is expensive, and carbon fiber reinforced polymers cost more than other fiber reinforced polymers (FRPs) such as glass or aramid, but they are stronger and more durable, and require minimal maintenance after installation. Engineers' concerns regarding durability have led to the selection of CFRP in many reinforced concrete applications in spite of its higher cost (Malvar, Warren, & Inaba, 1995). Table 1-1 and Table 1-2 show the typical tensile properties of fibers and FRP laminates.

Table 1-1 Typical tensile properties of fibers used in FRP systems (ACI 440.2R-17)

Fiber Type	Elastic Modulus	Ultimate Strength	Rupture Strain
Carbon Fiber	33000-34000 (ksi) 227.52-234.42 (GPa)	550-700 (ksi) 3.79-4.83 (GPa)	0.014
Glass Fiber	10000-10500 (ksi) 68.94-72.39 (GPa)	270-390 (ksi) 1.86-2.69 (GPa)	0.045
Aramid Fiber	16000-18000 (ksi) 110.32-124.10 (GPa)	500-600 (ksi) 3.45-4.14 (GPa)	0.016

Table 1-2 Typical tensile properties of FRP laminates (ACI 440.2R-17)

Fiber System (w/epoxy)	Elastic Modulus	Ultimate Strength	Rupture Strain
Carbon Fiber	15000-21000 (ksi) 103.42-144.78 (GPa)	150-350 (ksi) 1.03-2.41 (GPa)	0.010-0.015
Glass Fiber	3000-6000 (ksi) 20.68-41.36 (GPa)	75-200 (ksi) 0.52-1.38 (GPa)	0.015-0.030
Aramid Fiber	7000-10000 (ksi) 48.26-68.95 (GPa)	100-250 (ksi) 0.689-1.72 (GPa)	0.020-0.030

By comparing the properties of FRP laminates and FRP fibers, it can be seen that the laminates have fewer tensile properties. In general, FRP bars have fiber volumes of

50 to 70%, precured systems have fiber volumes of 40 to 60%, and wet lay-up laminate systems have fiber volumes of 25 to 40%. Because the fiber volume influences the gross laminate properties, precured laminates usually have higher mechanical properties than laminates created by using the wet layup technique. (ACI 440.2R)

Previously, steel plates, post-tensioning, and section enlargements were most often employed to strengthen structures, but externally bonded CFRP recently has become a popular method for strengthening and protecting concrete. Externally bonded CFRP is a superior repairing technique; however, it has the disadvantage of debonding, which may occur at less than 50% of the CFRP tensile strength capacity, which implies that half of its tensile capacity is ineffective (Orton et al., 2008). Past studies showed that the use of mechanical anchors, fan anchors, and u-wraps assist in mitigating the debonding and utilizing the maximum capacity of the CFRP (Anil and Belgin, 2010; Elsafty et al., 2013). Interestingly, no studies have investigated the application of presaturated CFRP to strengthen reinforced concrete structures exposed to harsh environments, such as bridges that have deteriorated due to concrete damage caused by impact, fire, corrosion, and/or an alkali-silica reaction. It is believed that this method will help to reduce the time and cost for repairing the damage.

1.2 Problem Statement

Preventing the corrosion of steel rebars embedded in concrete is one of the most challenging facets of concrete bridge maintenance that faces highway departments today. The deterioration of bridge columns is often caused by the corrosion of embedded steel reinforcements because of their long term exposure to chloride, water, and oxygen. Many bridges are built in and around coastal areas, and their exposure to marine water puts them at high risk for corrosion (Figure 1-3).

Figure 1-3 Bryant Patton Bridges displaying reinforced concrete piles with significant corrosion induced damage-Florida. (D.V.Reddy,2006)

In reinforced concrete bridge substructures that are exposed to marine water in coastal environments, the steel rebars are shielded by the alkaline nature of the peripheral concrete. However, the chloride ions that accumulate on the surface of the concrete slowly penetrate the concrete cover and reach the reinforcing steel. When the rate of chloride ion concentration at the steel rebar depth surpasses a critical threshold value, the protective passive layer on the steel surface breaks down, and active corrosion of the steel begins. The corrosion products occupy a volume that can be several times larger than that of the initial steel, thus causing cracks of the concrete cover that lead to structural damage. The time period from construction to the beginning of active rebar corrosion is called the initiation stage of the corrosion process. The following period, from the beginning of active corrosion until the appearance of an external manifestation of structural damage (cracking, rust, spalling), is called the propagation stage. Previous studies on CFRP focused on enhancing the ductility and strength of concrete structures by employing the CFRP wrapping technique to lower the rate of corrosion. None of the research investigated presaturated CFRP-wrapped concrete. Therefore, the primary objective of this research is to experimentally and analytically investigate the effects of using presaturated CFRP-wrapped concrete on water permeability and chloride ingress. This investigation was aimed primarily at determining the extent of corrosion experienced

during the propagation stage in marine substructures of coastal bridges.

1.3 Objectives

The effectiveness of the CFRP wrap depends on various parameters such as the type of fiber, orientation of the fiber, partially wrapped fibers versus unwrapped fibers, the number of CFRP layers, and the type of matrix. This study will experimentally and numerically examine the chloride ingress and water permeability of presaturated CFRP-wrapped concrete specimens and will determine the percentage of reduction that will lower the rate of corrosion. For the experimental study, ASTM C1152 (2012) will be used to determine the amount of chloride in concrete or mortar by using nitric acid to free the acid- soluble chloride and cause a chemical titration. The ASTM C1585 (2013) method will be employed to measure the rate of water absorption of both the concrete surface and interior concrete. The numerical study will be conducted using ANSYS in two phases. In the first phase, the model will be calibrated, using the experimental result. In the second phase, the parameters, such as the number of CFRP layers, the control samples without a CFRP layer, and high permeability concrete, will be varied.

1.4 Methodology

This research involves preparing the samples, simulating the corrosion resistance, repairing the concrete, strengthening the concrete with presaturated CFRP, and calibrating the 2-D cylindrical model specimen. The research methodology is as follows:

1. Model a 2-D (half-circle) of concrete using Ansys software.
2. Examine the chloride diffusion and water diffusion in the concrete.
3. Validate and compare the performances of the control specimen, regular CFRP, and pre-saturated CFRP-wrapped concrete.
4. Perform a parametric study and calibrate a 2D finite element model of the control specimen, regular CFRP, and presaturated CFRP.

1.5 Organization of the Thesis

This thesis is organized into five chapters. The content of each chapter is as follows.

Chapter 2: Literature Review

This chapter presents a review of previously conducted experimental and numerical studies on the effect of chloride ingress and water permeability of concrete wrapped with CFRP.

Chapter 3: Sample Preparation

This chapter discusses the preparation of the samples, the patching of voids, and wrapping of CFRP on concrete specimens.

Chapter 4: Experimental Procedure

This chapter discusses the chloride penetration experimental tests that were conducted on cylindrical concrete specimens that were in a saline solution for 42 days. The water penetration of a concrete cylindrical specimen immersed in water for 9 days is also discussed.

Chapter 5: Experimental Results

The results of the experimental tests obtained from performing ASTM C 1583 and ASTM C 1152 tests are described in this chapter. The results were obtained from a control specimen, Sika Hex 107 (regular CFRP), and Sika 117 C (presaturated CFRP).

Chapter 6: Numerical Modeling

This chapter discusses the numerical modeling performed to verify the response of the 2-D study of water permeability and chloride ingress.

Chapter 7: Parametric Study

This chapter discusses the parametric study of a TxDOT bridge column was performed to verify the response of the 2-D study of water permeability and chloride ingress.

Chapter 8: Numerical Results

This chapter discusses the results of the numerical tests performed on water absorption and chloride ingress, using ANSYS APDL software. A numerical model was developed, based on the laboratory test results, to verify the numerical study. An extensive parametric study of a TxDOT column was conducted to identify the deterioration level of CFRP and the threshold limit of the clear cover.

Chapter 9: Summary, Conclusions and Recommendations

The summary of the research conducted is presented in this chapter, and the conclusions drawn from the experimental chloride penetration test, water permeability test, and numerical modeling are outlined. Recommendations for further research are discussed.

Chapter 2

Literature Review

Ashour et al (2018) conducted an experimental investigation of the effect of changing the type of FRP on the lateral response of reinforced masonry columns (RMC) under quasistatic cyclic loading. The results indicated that CFRP-upgraded RMC showed higher strength and ductility than GFRP. Limited studies were conducted on the effect of FRP wrapping on concrete chloride ingress.

Rafaat and Mark (2010) simulated various harsh environments to study the effect of environmental conditions on concrete cylinders wrapped with FRP. Some of the cylinders that were subjected to heating and cooling were later subjected to freezing and thawing cycles, while others were submerged in fresh water or salt water. The specimens were loaded to failure under a uniaxial compressive load, and the axial and lateral deformations were monitored. The results indicated that the strength of the FRP-wrapped cylinders increased by 43-74% over the unconfined concrete cylinders under heating and cooling, and freezing and thawing cycles. Exposure to fresh or salt water had a slightly negative effect on the compressive strength, and exposure to high temperatures had no effect on the strength of the wrapped concrete cylinders.

Yazdani and Gracia (2014) investigated the effectiveness of applying FRP wrapping on concrete surfaces to reduce the ingress of chloride and increase durability. They studied nine specimens that had been exposed to sodium chloride for six weeks. The results indicated that both types of FRP wrapping resulted in a significant reduction in chloride penetration.

Yazdani and Goucher (2015) looked at the effectiveness of FRP wraps in reducing chloride ingress and increasing durability of lightweight concrete. The studies investigated 42 cylinders that had been subjected to electricity-induced accelerated testing in a saline solution for 50 days. Results showed that multiple wraps were more

effective at reducing chloride ingress than single wraps, and CFRP-wrapped lightweight concrete demonstrated longer durability.

Yazdani et al (2017) studied the effect of various FRP wrapping parameters such as type, fiber orientation, role of epoxy adhesive, and number of layers. They investigated 12 cube specimens that had been immersed in a surface saline pond for 16 weeks. The results indicated that the chloride content decreased rapidly and linearly with the penetration depth and that external FRP wrapping provides an excellent barrier to chloride ingress (28% reduction on average).

Sangeeta et al. (2009) studied whether FRP overlays enhance the compressive strength of concrete columns experiencing the same corrosion rate as that of unwrapped columns, due to the confinement that is provided when fibers are oriented in the hoop direction and delay cracking of the concrete cover. It is not clear whether FRP wraps reduce the corrosion rate in reinforcing bars after corrosion commences or simply delay the cracking time. Since FRP overlays can reduce the diffusion of harmful ions such as chloride into the concrete, they can increase the time it takes for the chloride concentration at the surface of reinforcing bars to reach the threshold value required to initiate corrosion.

Weitsman, Y. (1977) investigated the effects of water on epoxy and mild steel joints, and found that the deprivation of joints could be defined as the attainment of a critical moisture status at the bond interface. Nguyen, T. (1998) measured the moisture status at the bond interface of an epoxy-covered concrete specimen and revealed that a few water molecule layers were present in the epoxy and concrete interface after the specimens had been exposed to water for certain duration.

Many researchers are investigating the diffusion of chloride in sound concrete and steel rebar corrosion. The diffusion process of chloride in concrete is slow and complex and involves many material and environmental variables （Kong et al. 2002).

Xi et al. (1999) developed a mathematical model to determine the chloride binding capacity for chloride penetration in saturated concrete. Based on finite differences methods and Fick's diffusion law, Conciatori et al. (2008) proposed a numerical model, TransChlor, to simulate the transport of chloride ions in concrete. After considering the effects of cement type, curing condition, and age, Guneyisi et al. (2009) proposed a neural network model-based formulation to predict the chloride permeability in concrete.

Chuanqing Fu et al (2010) studied a modified chloride ions diffusion model with cracks in the concrete and performed an FEM analysis in ANSYS. The results were compared with the test results presented by Wittmann (2008) and showed that the new mathematic model was able to predict the chloride diffusion depth in cracked concrete with good accuracy.

Ouyang, Z. and Wan, B. (2008), conducted an experimental study to investigate the relation between the bond interface region, relative humidity, and fracture energy of FRP and concrete bond joints. The results showed that the relative humidity of the interface region was a primary factor in the bond fracture energy of FRP and concrete specimens in a moist environment. The results revealed a highly uneven moisture distribution along the adhesive, especially for a relatively short period of exposure, which caused an even distribution of its mechanical properties. The moisture accumulated in the interface came primarily from the bond-free area close to the FRP and the sides of the specimen. Higher relative humidity (RH) increased not only the (RH) at the given exposure time, but also the wetting speed.

FRP systems are applied in four forms: wet layup systems, prepreg systems (presaturated), precured systems, and near-surface-mounted systems (ACI Committee 440R, 2017). In wet layup, the FRP sheets are saturated with resin on-site and then applied to the concrete surface and cured in place. There are two procedures for wet layup systems. One is to saturate the FRP with resin and then apply it directly to the

concrete surface; the other is to apply it first to the concrete surface and then saturate it with the resin, using a roller.

Presaturated CFRP differs from wet layup, as the presaturated CFRP is already saturated with resin, which saves labor, time, and cost. A lot of research has been conducted on regular CFRP, while limited research has been conducted on presaturated CFRP. Pandey (2018) compared the performance of presaturated and regular CFRP unreinforced concrete beams and found that the failure loads of the beams strengthened with presaturated and regular CFRP increased by 78% and 62%, respectively, compared to that of the control beam that had not been strengthened. Despite all of the FRP advantages, it also has disadvantages, such as brittle failure, poor shear resistance, poor resistance to fire, and bonding failure (Masuelli, 2013).

Past studies primarily focused on the use of the CFRP wrapping technique to lower the rate of corrosion in reinforced concrete structures to increase durability. However, none of the research investigated presaturated-CFRP-wrapped concrete. Therefore, the primary objective of this research is to experimentally and analytically investigate the effects of water permeability and chloride ingress on concrete wrapped with presaturated CFRP.

Chapter 3

Sample preparation

Normal strength concrete (grade 3000 psi) and high strength concrete (grade 6000 psi) at 28 days from normal ordinary Portland cement were prepared. Figure 3-1 shows 9 concrete cylinders with a 100 mm (4 in) diameter and 200 mm (8 in) height: five with 3 ksi (20.68 MPa) and four with 6 ksi (41.36 MPa). Before they were wrapped with the CFRP, the concrete specimens were spliced into two halves, as shown in Figure 3-2, then were each spliced into four pieces (100 mm in diameter x 50 mm in thickness). Among these 32 specimens, 12 were wrapped with single-layer regular carbon FRP (Sika Wrap Hex 103 C), 12 were wrapped with single-layer presaturated CFRP (Sika Wrap 117 C), and 8 served as control specimens. The cylinders were tested for water permeability and chloride ingress.

Figure 3-1 Casting of concrete cylinders

Figure.3-2 Test specimens before CFRP wrapping

3.1.1 Design Mix

The concrete used in this study was made in two batches. Cow town Redi Mix Concrete, Fort Worth, Texas supplied a batch of 3000 psi concrete (batch 1) and 6000 psi concrete (batch 2).

Table 3-1 Design mix for concrete grade 3000 psi (20.68 MPa)

Component	Value
W/C ratio	0.244
1" Limestone	1850 lb (839.14 kg)
Sand1	336 lb (152.40 kg)
Man sand	1001 lb (454.04 kg)
Cement	414 lb (187.78 kg)
Flyash	103 lb (46.72 kg)
Water	29.5 gal (111.62 L)
Sika plastiment	10.3 Oz (0.292 kg)
Sika air	20.7 Oz (0.589 kg)

Table 3-2 Design mix for concrete grade 6000 psi (41.36 MPa)

Component	Value
W/C ratio	0.196
1" Limestone	1850 lb (839.14 kg)
Sand1	315 lb (142.88 kg)
Man sand	938 lb (425.46 kg)
Cement	583 lb (264.44 kg)
Flyash	146 lb (66.22 kg)
Water	31 gal (117.35 L)
Sika plastiment	14.6 Oz (0.413 kg)
Sika air	51 Oz (1.44 kg)

3.1.2 CFRP

SikaWrap-103, a unidirectional woven carbon fiber fabric, was applied. It is a high-strength carbon fiber that generally comes in a one-roll package with 91400 mm/roll (3598.42 in/roll) and 635 mm (25 in) width, as shown in Figure 3-3. Similarly, SikaWrap-117 C, a unidirectional presaturated CFRP wrap was applied. It comes in a one-roll package with 91400 mm/roll (3598.42 in/roll) and 600 mm (23.62 in) width, as shown in Figure 3-4.

Figure 3-3 SikaWrap Hex 103 C

Figure 3-4 SikaWrap Presaturated 117 C

The detailed characteristics of the CFRP and presaturated CFRP are presented in Table 3-3 and Table 3-4.

Table 3-3 Dry fiber properties of CFRP (SikaWrap Hex 103 C)

Typical Dry Fiber Properties			
Tensile Strength		550 ksi (3,793 MPa)	
Tensile Modulus		34 msi (234.5 GPa)	
Ultimate Elongation		1.5%	
Density		18 oz. / sq. yd. (610 g/m2)	
Thickness		0.0135 in. (0.34 mm)	
Composite Gross Laminate Properties			
Nominal Ply Thickness		0.04 in. (1.0 mm)	
Property	**ASTM Method**	**Typical Test Value**	**Design Value***
Tensile Strength	(ASTM D 3039)	181.0 ksi (1,248 MPa)	160.9 ksi (1,110 MPa)
Tensile Modulus	(ASTM D 3039)	-	10.39 msi (71.7 GPa)
Tensile % Elongation	(ASTM D 3039)	1.75%	1.45%
Tensile Stiffness	(ASTM D 7565)	-	416 kips/in. width (74,289 kg/cm width)

3.1.3 Epoxy

The epoxy used was Sikadur-330, which comes with a hardener (part B) and resin (part A). Three types of epoxy resins were used with the CFRP, namely epoxy, vinyl ester, and polyester. Each type has distinct characteristics and functions; however, epoxy resin was used because it has higher (threefold) strength than vinyl ester and polyester. Epoxy adheres well to CFRP and forms a leak-proof barrier. Epoxy resin exhibits outstanding mechanical properties, good handling characteristics, and minimum shrinkage after curing (Table 3-5), and shows high resistance to water and chemical attacks [18]. Part A epoxy resin is paste-like in consistency and white, whereas part B is paste-like and grey. When mixed together, the parts produce a light grey mixture. Parts A and B epoxy come in 24 and 6 kg per pail, respectively. The shelf life of epoxy is 2 years

from the date of manufacturing if it is packed appropriately in its prototype, unopened, placed in a dry environment at temperatures not exceeding +30 ^{0}C, and protected from direct daylight, as shown in Figure 3-5 . The physical and mechanical properties of epoxy are displayed in Table 3-6. The CFRP was cured up to 35 °C on the 2nd day (Table 3-5).

Table 3-4 Presaturated fiber properties of CFRP (SikaWrap Hex 117 C)

Typical Presaturated Fiber Properties			
Density		0.065 lbs./in^3 (1.8 g/cc)	
Mass per Unit Length		9 oz. / sq. yd. (300 g/m^2)	
Composite Gross Laminate Properties			
Property	ASTM Method	Cured Properties	Design Value
Nominal Ply Thickness	-	0.019 in (0.48 mm)	0.018 in (0.48 mm)
Tensile Strength	(ASTM D 3039)	119,770 psi (825 MPa)	93,662 psi (645 MPa)
Tensile Modulus	(ASTM D 3039)	-	8,973,997 psi (61,873 MPa)
Tensile % Elongation	(ASTM D 3039)	1.22 psi (1.22 MPa)	1.04 psi (1.04 MPa)
Tensile Stiffness	(ASTM D 7565)	-	170.5 kips/in. width psi
Tensile Resistance	-	5.17 kips/in. width	1.78 kips/in. Width

Table 3-5 CFRP curing details

Temperature	Full Cure
+10 °C	7 days
+10 °C	5 days
+10 °C	2 days

Figure 3-5 Epoxy resin (Parts A and B) were mixed using an electric paddle.

3.2 Concrete surface preparation before FRP installation

Both ACI 440 (2008) and the FRP manufacturer require that the substrate surface, to which the FRP adheres, be a concrete surface Profile 3 (CSP 3) as specified by the International Concrete Repair Institute (ICRI). ICRI's guideline specifies nine distinct surface profiles ranging from CSP 1 to CSP 9, as depicted in Figure 3-6. For the current study, the surface preparations were done with a handheld air needle scaling tool to get the required surface profile CSP 3 (Figures 3-7 a, b & c). A blower was used to remove dust or loose material from the concrete's surface.

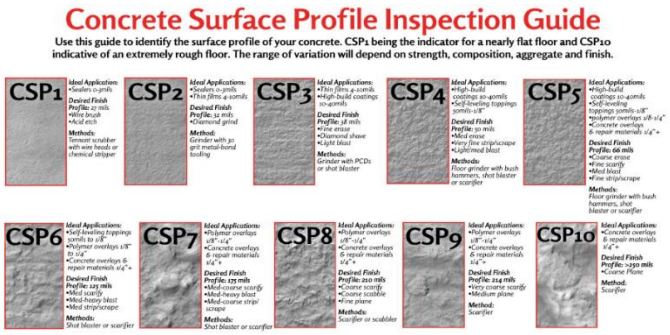

Figure 3-6 ICRI concrete surface profiles (CSP) (Runyon surface prep)

(a) Before grinding with air needle scaling tool

(b) After grinding

(c) Air needle scaling tool with CSP-3

Figure 3-7 Concrete cylinder specimens before and after grinding

Mixing of Sikadur 31

Each component was mixed by combining one part component B with one part component A (1:1) by volume in a clean pail or other appropriately sized mixing container and mixing thoroughly for 3 minutes, until the mixture was uniform in color Figure 3-3 (d). The quantity mixed had to be used within its pot life (60 minutes at 73 °F). As shown in Figure 3-8 (e), Sikadur 31 Hi- Mod gel was used to patch any voids or honeycombs on the surface of the concrete.

(d) Mixing of Sikadur 31

(e) Patching of voids

Figure 3-8 Patching of voids using Sikadur 31

(f) After patching

(g) Wrapping CFRP

Table 3-6 Physical and mechanical properties of epoxy (Sika)

Chemical base	**Epoxy Resin**
Density	1. 25 gal. (4.7 L) Part A + 0.35 gal. (1.3 L) Part B mixed at +23^{o} C
Viscosity	Shear rate: 50/s +10^{o}C ~ 10000 mPas +23^{o}C ~ 6000 mPas +35^{o}C ~ 5000 mPas
Thermal Expansion Coefficient	4.5 x 10^{-5} per ^{0} C (-10^{o} C to +40^{o} C)
Tensile Strength	30 Ma (7 days at +23^{o} C)
Bond Strength	Concrete Fracture (> 4 MPa)
Elastic Modulus	Flexural:3800 MPa (7 days at 23^{0} C) Tensile :4500 MPa (7 days at 23^{0} C)
Elongation at Break	0.9% (7 days at +23^{o} C)
Chemical Resistance	Not suitable for chemical exposure
Thermal Resistance	Continuous exposure +45^{o}c

Chapter 4

Experimental Procedure

4.1 Chloride Penetration Test Procedure (ASTM C1152)

For the chloride penetration testing, 16 specimens were placed in a plastic tank with dimensions of 664 mm (26 1/8 in) x 413 mm (16 1/4 in) x 343 mm (13 1/2 in) he specimens were submerged up to approximately 3¼ (in) of a 5% by weight salt solution that was made by combining distilled water with ordinary table salt, as shown in Figure 4-1. The ASTM C1152-12 procedure, Standard Test Method for Acid-Soluble Chloride in Mortar and Concrete, was followed, and the concrete samples were drilled using a rotary impact drill to collect 20 gm of powered material, as shown in Figure 4-2. Ten (10) gm were transferred to a 0.0660 US gal (250 mL) beaker (Figure 4-3) and diluted with 0.0198 US gal (75 mL) of deionized water, as shown in Figure 4-4. Then 0.0660 US gal (25mL) of 1:1 nitric acid with a normality of 30.283 mol/US gal (8 mol/L) was added slowly, as shown in Figure 4-5. Three drops of methyl orange indicator were added and mixed as shown in Figure 4-6. If the solution did not turn pink, a small amount of nitric acid was added drop-by-drop, until a pink color appeared. Once the pink or reddish color persisted, 0.00264 US gal (10 mL) drops of nitric acid were added and the beaker solution was brought to a boil and immediately removed from the hot plate. The sample was filtered through a 9 cm coarse textured filter paper in a 0.0660 US gal (250 mL) Buchner funnel. The beaker and the filter paper were rinsed twice with small portions of water, and the filtrate was transferred from the flask to a 0.0660 US gal (250 mL) beaker. The filtrate was cooled to room temperature. The volume did not exceed 0.0460 US gal (175 mL). For instruments equipped with a dial readout, it was necessary to establish an approximate equivalence point by immersing the electrodes in a beaker of water and adjusting the instrument to read about 20 mV lower than mid-scale. The approximate millivoltmeter reading was recorded, the beaker was removed, and the electrodes were wiped with absorbent paper. A standardized NaCl solution with a normality of 0.0946 mol/US gal

(0.025 mol/L), 0.00028 US gal (2.0 mL) was transferred into the beaker. The beaker was placed on a magnetic stirrer, as shown in Figure 4-7, and the electrodes were immersed in the solution, making sure that the stir bar did not touch the electrode.

The delivery tip of the filled 0.00264 US gal (10 mL) buret was placed to the zero mark with standardized 0.05 N AgNO3 .To begin the titration process, the amount of standard 0.05 N silver nitrate solution required to bring the millivoltmeter reading to -60.0 mV of the equivalence point determined in the water was recorded (ASTM C114-18). The titration was continued in 0.00005283 US gal (0.20 mL) increments. The change in mV was then calculated as shown in column 3. The equivalence point is the maximum change in mV value from column 3, as shown in column 4. The equation following the recorded values in Table 4-1 was used to determine the equivalence point.

Titration continued until three readings past the approximate equivalence point were recorded. The precise equivalence point of the titration was calculated, and the results of the water blank were subtracted.

$$CL\% = 3.45\left[\left(\frac{V_1 - V_2}{W}\right)N\right] \qquad (1)$$

Where,

V_1 = mL of 0.05 N AgNO solution used for sample titration (equivalence point)

V_2 = mL of 0.05 N AgNO solution used for blank titration (equivalence point)

N = normality of the 0.05 N $AgNO_3$ solution &

W = mass of sample in (g)

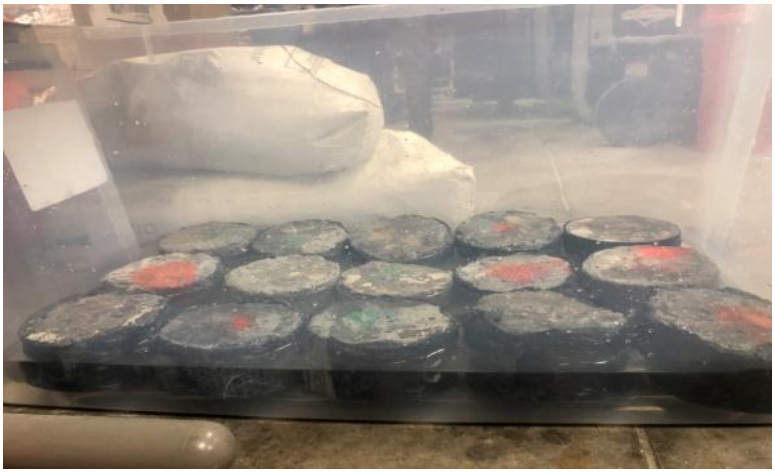

Figure 4-1 Salt ponding

Figure 4-2 Concrete samples drilled using rotary impact drill, collecting approximately 10 g of powdered material.

Figure 4-3 Powdered sample

Figure 4-4 Reagent water poured into beaker

Figure 4-5 Nitric acid being added into beaker

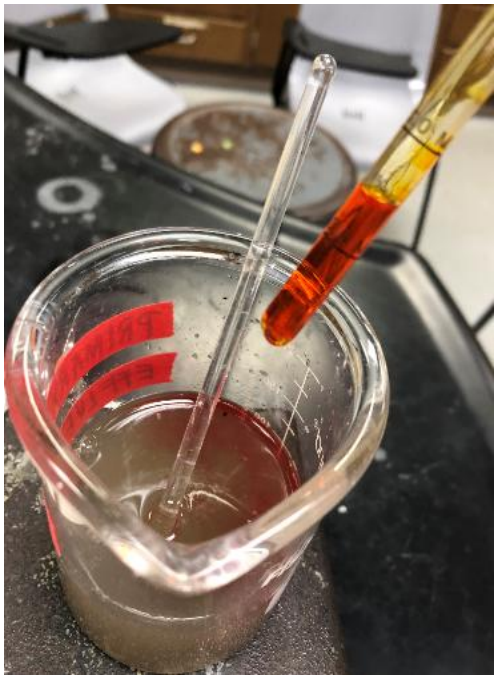

Figure 4-6 Added methyl orange indicator

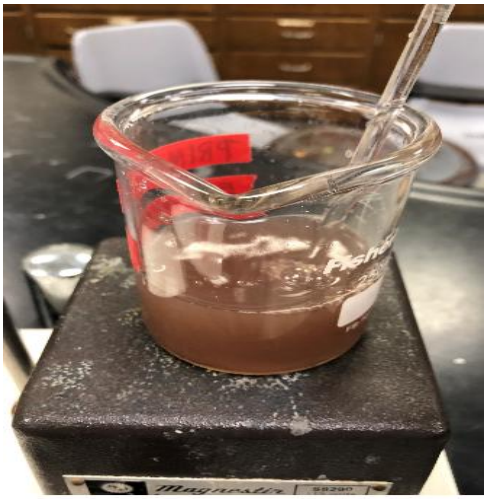

Figure 4-7 Mixing samples using glass and magnetic stirrer

Table 4-1 Method for determining the equivalence point (ASTM C 114-18)

Equivalence Point Determination ASTM C 114			
AgNO3 (mL) (Column 1)	Potential (mV) (Column 2)	ΔmVA (Column 3)	Δ2mVB (Column 4)
1.6	125.3		
		5.8	
1.8	119.5		1.4
		7.2	
2.0	112.3		1.3
		8.5	
2.2	103.8		1.3
		9.8	
2.4	94		0.6
		9.2	
2.6	84.8		2.3
		6.9	
2.8	77.9		0.8
		6.1	
3.0	71.8		1.3
		4.8	
3.2	67		
The equivalence point is in the maximum Δ mV interval (Column 3) and thus between 2.20 and 2.40 mL. The exact equivalence point in this 0.20 mL increment is calculated from the Δ mV (Column 4) data as follows: $$E = 2.20 + \left(\frac{1.3}{1.3 + 1.6}\right) * 0.2 = 2.337\ ml \rightarrow round\ to\ 2.34ml$$			
A Differences between successive readings in Column 2			
B Differences between successive Δ readings in Column 3			

4.2 Water Absorption Test Procedure (ASTM C1585)

This test method is used to measure the water absorption rate of both the surface and interior of the concrete. The size specimen recommended by ASTM C1585 (2013), Standard Test Method for Measurement of Rate of Absorption of Water by Hydraulic-Cement Concretes, was used for the test.

Figure 4-8 Water absorption test setup

One surface was exposed to 1± 2 mm (0.0393 ± 0.0787 in) of room temperature water. The sides were sealed with candle wax, and the top surface was covered by a plastic sheet, as shown in Figure 4-8. The determination of mass was recorded at regular intervals. Table 4-2 shows the times and tolerances for the measurement schedule.

Absorption, I, is the change in mass divided by the product of the cross-sectional area of the test specimen and the density of water.

$$I = \frac{m_t}{a * d} \qquad (2)$$

Where,

I = the absorption,

m_t = the change in specimen mass in grams, at the time t,

a = the exposed area of the specimen, in mm^2, and

d = the density of the water in g/mm^3.

TABLE 4-2 Times and tolerances for the measurements schedule

Time	Tolerance
60 s	2 s
5 min	10 s
10 min	2 min
20 min	2 min
30 min	2 min
60 min	2 min
Every hour up to 6 h	5 min
Once a day up to 3 days	2 h
Days 4 to 7	2 h
Days 7 to 9	2 h

Chapter 5

Experimental Results

5.1 Water permeability test results

All of the cylinders, except the control samples, were wrapped with a single layer of CFRP and presaturated CFRP. The water permeability of the normal strength and high strength graded concrete wrapped with CFRP laminate was analyzed.

Table 5-1 Water permeability test for control, regular, and presaturated CFRP

	I=ΔM/area*density of water (mm)					
Time (S)^1/2	Control Normal Strength	Control High Strength	Regular CFRP Normal Strength	Regular CFRP High Strength	Presaturated CFRP Normal Strength	Presaturated CFRP High Strength
0	0	0	0	0	0	0
8	0.1234	0.1233	0	0	0	0
17	0.2467	0.2467	0	0	0	0
24	0.37	0.37005	0.4488	0.1632	0	0
35	0.37	0.37005	0.4896	0.1632	0	0
42	0.4934	0.4934	0.5304	0.1632	0	0
60	0.6168	0.4934	0.5712	0.1632	0	0
85	0.7401	0.5597	0.5712	0.1632	0	0
104	0.8018	0.61675	0.5726	0.204	0	0
120	0.9251	0.6784	0.5756	0.2448	0	0
134	1.1102	0.74005	0.5726	0.2856	0	0
147	1.2335	0.80175	0.5712	0.3672	0.0408	0
300	2.0353	1.26345	0.8976	0.5712	0.0408	0
420	2.3437	1.44845	0.8976	0.5712	0.0408	0
520	2.652	2.1718	0.9001	0.5712	0.1224	0
569	3.0838	2.29515	0.8976	0.5712	0.1632	0
668	3.2155	2.32685	0.9416	0.5712	0.2040	0.0408
722	3.4407	2.37135	1.0308	0.612	0.2448	0.0408
789	3.5155	2.40685	1.1016	0.612	0.3264	0.0408
829	3.6388	2.48015	1.1832	0.612	0.3672	0.0408

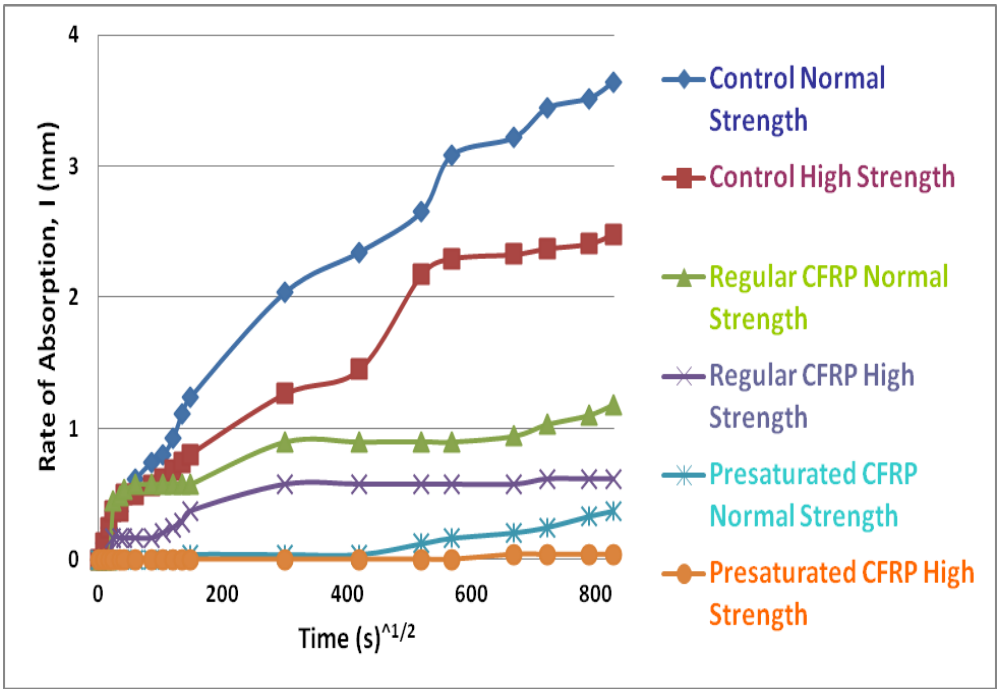

Figure 5-1 Water absorption plot for control specimen, regular CFRP, and presaturated CFRP

The purpose of a water permeability test is to measure the rate of water that could penetrate the concrete. Table 5-1 and Figure. 5-1 show that the absorption of water was reduced in the presaturated CFRP-wrapped concrete. The average penetration of normal strength concrete and high strength concrete control cylinders was approximately 3.64 mm (0.143 in) and 2.48 mm (0.097 in), respectively. The rates of absorption of normal strength regular CFRP, high strength regular CFRP, normal strength presaturated CFRP, and high strength presaturated CFRP layer were 1.18 (0.046), 0.61(0.024), 0.36 (0.014), and 0.04 (0.0015) mm (in), respectively.

The diffusion coefficient (k) for the regular CFRP and presaturated CFRP obtained for this study were from the water absorption test. The average water permeability coefficients recorded for the regular CFRP (normal and high strength) and presaturated CFRP (normal and high strength concrete) were approximately 1.324×10^{-4}

(2.118 x 10^{-7}), 5.63x10^{-4} (9.008 x 10^{-7}), and 7.31x10^{-7} (1.169 x 10^{-9}), and 3.60x10^{-8} (5.76 x 10^{-11}) mm^2/s (in^2/s), respectively. The CFRP wraps afforded a barrier for the water permeability of the tested specimens, and minimum penetration was found in those areas wrapped with presaturated CFRP. Therefore, it can be concluded that CFRP wraps are effective at reducing corrosion caused by water permeability.

5.2 Chloride ingress test results

The results that were obtained after performing ASTM C 1152 test on the Sika 117 C (presaturated CFRP), Sika Hex 103 (regular CFRP), and control specimens are shown in Table 5-2.

Table 5-2 Chloride permeability test for control, regular, and presaturated CFRP results obtained from each sample at each depth

Specimen	Depth (mm)	Chloride (%)
Presaturated CFRP (PCFRP-NS)	7.5	0.083
Regular CFRP (RCFRP-NS)	7.5	0.180
Control (CNS)	7.5	0.376
Presaturated CFRP (PCFRP-NS)	12.5	0.067
Regular CFRP (RCFRP-NS)	12.5	0.146
Control (CNS)	12.5	0.285
Presaturated CFRP (PCFRP-NS)	25	0.053
Regular CFRP (RCFRP-NS)	25	0.128
Control (CNS)	25	0.236
Presaturated CFRP (PCFRP-HS)	7.5	0.044
Regular CFRP (RCFRP-HS)	7.5	0.136
Control (CHS)	7.5	0.281
Presaturated CFRP (PCFRP-HS)	12.5	0.036
Regular CFRP (RCFRP-HS)	12.5	0.116
Control (CHS)	12.5	0.239
Presaturated CFRP (PCFRP-HS)	25	0.016
Regular CFRP (RCFRP-HS)	25	0.093
Control (CHS)	25	0.198

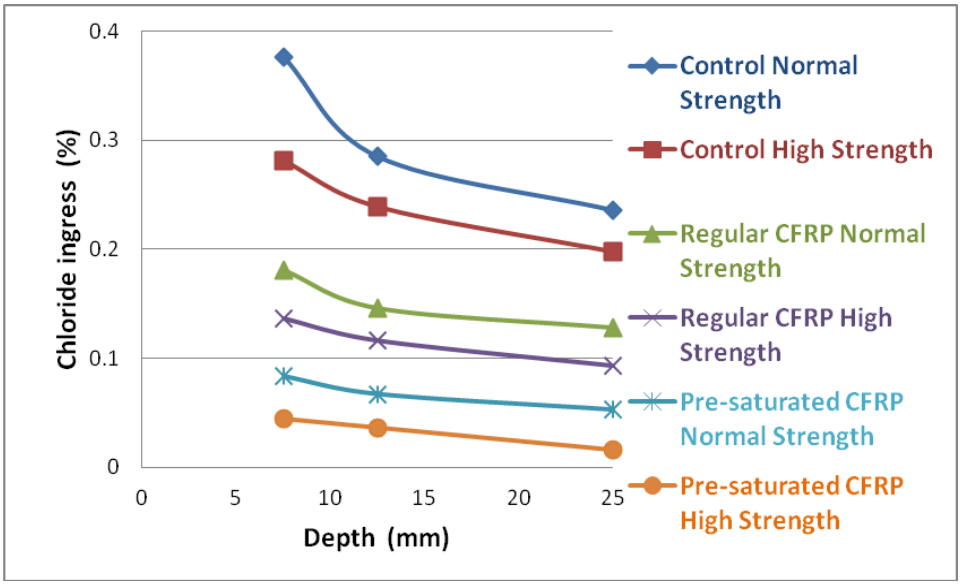

Figure 5-2 Chloride ingress plot for contol specimen, regular, and presaturated CFRP

Table 5-2 and Figure 5-2 show the chloride content of the regular CFRP-wrapped normal and high strength concrete, presaturated CFRP-wrapped normal and high strength, and normal and high strength concrete control specimen. The normal and high strength presaturated CFRP showed the smallest amount of acid soluble chloride for the single layer Sika presaturated CFRP configuration. The chloride content was highest in the normal and high strength concrete control specimens. All of the samples showed lower amounts of chloride when they were wrapped with CFRP, and the percent of chloride in the presaturated CFRP specimens was lower than in the regular CFRP and control specimens at every depth. However, at 25 mm depth, the reduction of chloride was lowest (less than 0.053% and 0.016%). This could be attributed to the length of time that the specimens were exposed to the sodium chloride solution, since, for this study, they were only exposed for six weeks. If the period of ponding had been longer, the results would have indicated different values for all of the depths. The chloride percentage at 7.5 mm had the highest rate of chloride reduction, and the presaturated CFRP provided a stronger barrier to chloride ingress than either the regular CFRP or the control specimen.

Chapter 6
Numerical Modeling

The numerical model was developed with ANSYS APDL (2013) finite element analysis software to verify the model response of the 2-D concrete problem of chloride ion diffusion and water movement diffusion. The numerical analysis consisted of three modeling steps: chloride diffusion, water diffusion analysis, and transient thermal analysis. The goal of these finite element analyses was to accurately determine the percentage of chloride content and moisture content with respect to time.

6.1 Introduction to finite element analysis

Finite element analysis (FEA) is a technique preferred by many researchers for exploring the behavior of structural materials and elements. It relies on the discretisation of the geometry to solve thermal equations, effectively subdividing the structure into smaller (finite) elements. The discrete model approximates the behavior of the real physical structure; however, if the discretisation mesh is dense enough, the approximation is sufficient to accurately model reality. This method produces quicker results than experimental investigations and is less expensive.

An attempt was made in this study to perform a nonlinear FEA to analyze the chloride and water ingress of the two-dimensional concrete problem encountered in the experimental work. A transient thermal analysis was carried out using Ansys software, to determine the temperature and other thermal quantities in a body due to different thermal loads. The accuracy and the convergence of the solution depend on many factors, such as the convergence criteria, mesh density, and the constitutive properties of the materials.

6.1.1 Types of elements used

ANSYS PLANE 77 is a higher order version of the 2-D, 4-node thermal element PLANE55. It has one degree of freedom, temperature, at each node. The 8-node

elements have compatible temperature shapes and are well suited to a model's curved boundaries such as CFRP wrapping. The 8-node thermal element is applicable to a 2-D, steady state, or transient thermal analysis.

The geometry, node locations, and coordinates system for this element are shown in Figure 6-1. The element is defined by eight nodes and orthotropic material properties. A triangular shaped element may be formed by defining the same node number for nodes K, L, and O.

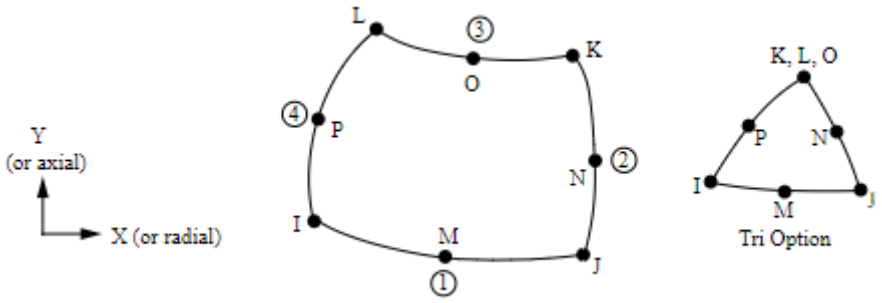

Figure 6-1 PLANE 77 geometry (ANSYS 2013)

6.1.2 Analytical model of control and CFRP-wrapped specimens

The analysis of the control and CFRP-wrapped cylindrical specimens was considered as a two-dimensional problem. The relative humidity varied with respect to place and time. The average environment of the NDE lab at the University of Texas at Arlington was recorded as having 45% humidity, as shown in Figure 6-2. Therefore, the 2-D cylindrical specimen analyzed had been exposed to 45% relative humidity.

Figure 6-2 Relative humidity recorded in NDE lab

6.1.3 Water permeability of concrete using regular and presaturated CFRP

A control specimen, a cylindrical specimen wrapped with regular CFRP, and a cylindrical specimen wrapped with presaturated CFRP were modeled in Ansys. A small half-circle area of the presaturated CFRP matrix was analyzed for water permeability. The meshed model is shown in Figure 6-3.) The dimensions of the model were 100 mm (3.93 in) diameter, regular CFRP/presaturated CFRP thickness of 1 mm (0.0393 in), and epoxy adhesive thickness of 1.2 mm (0.0472 in). The model was analyzed with 45% of relative humidity to look at the pattern of water movement. Table 6-1 shows the diffusion coefficients for epoxy and concrete.

Table 6-1 Diffusion coefficients with relative humidity (Ouyang, Z. and Wan, B., 2008)

Element	Diffusion Coefficient (m^2/s)	Relative Humidity (%)
Concrete	0.05×10^{-12}	45
Epoxy	10.00×10^{-14}	45

The diffusion coefficient of concrete is constant until 70 °C temperature is reached, and it rises from 70 °C to 90 °C. Beyond 90 °C, it remains constant. The epoxy

diffusion coefficient decreases with time. The FRP diffusion coefficient is not dependent on temperature, so has only one value (Ojha,2012).

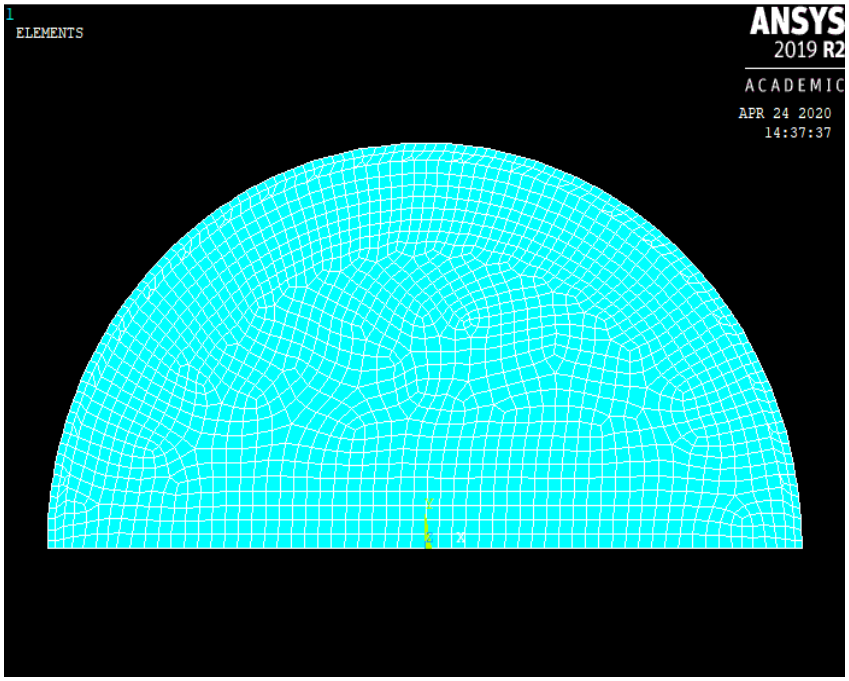

Figure 6-3 Meshed model (Control without CFRP)

6.1.4 Chloride Ingress of concrete using presaturated CFRP

The finite element method was used to simulate the chloride diffusion in concrete. Thermal analysis results proved to be sufficiently precise. In Finite element analysis, the chloride diffusion analyses is considered as a transient heat conduction problem and replace the boundary temperature and heat conductivity with chloride concentration and diffusion coefficient respectively. In this study's two-dimensional problem, the numerical model dimensions were 100 mm (3.93 in) diameter, regular CFRP/presaturated CFRP thickness of 1 mm (0.0393 in), and epoxy adhesive thickness of 1.2 mm (0.0472 in). The ANSYS PLANE55 element type was used to model the concrete.

The element has one degree of freedom, temperature, at each node. Chloride diffusivity (D_c) is calculated by the model in Life 365, according to the water to cement ratio (w/c) (Chuanqing Fu, 2010).

$$D_c = 3600*10^{-12.06+2.4(w/c)} \quad (4)$$

Where,

Surface chloride concentration C_s is 0.396 kg/m^3.

W/c is the water and cement ratio

Table 6-2 Diffusion coefficient based on w/c ratio

W/c ratio	Diffusion Coefficient (m^2/s)
0.244	1.219 x 10-^{8}
0.196	9.253 x 10-^{9}

Chapter 7
Parametric Study

7.1 Parametric study on a typical TxDOT column

A parametric study was conducted to determine the various factors that affect the durability of CFRP-wrapped reinforced concrete structures in marine environments. These parameters include the tensile modulus of CFRP, high permeable concrete (HPC), and the thickness and number of layers. To understand the effects of these parameters, a water permeability and chloride penetration parametric study was performed on a typical TxDOT 2-D circular column. Due to the limitations of the study, the effects of temperature variations were not incorporated into the modeling scheme, and the study was confined to considering constant full submersion, without taking tidal effects into account.

HPC seems particularly useful for protection against corrosion of reinforcing steel due to its low diffusivity and low permeability. The average diffusion coefficient (D_c) of R2M1 was 1.81 x 10^{-12} m^2/s (1.95 x 10^{-11} ft^2/s) [17]. The corrosion consultant uses a lower and more traditional value of 0.030% by weight of concrete, and Virginia Department of Transportation (VDOT) recommends a higher value of 0.080% [31]. Glass and Buenfeld (1997) summarized the threshold values reported in various studies as a range from 0.17% to 2.2% by weight of cement for field structures. With the same assumptions as those made by Glass and Buenfeld (1997), i.e., a cement content of 590 lb/yd3 and a concrete weight of 3,879 lb/yd3, the reported threshold value would range from 0.026% to 0.33% by weight of concrete. This difference can most likely be attributed to variability in the service conditions, concrete, and even reinforcing steel (Glass and Buenfeld, 1997; Li and Sagues, 2001; Stratfull et al., 1975). Other researchers have produced estimates for the chloride threshold value that range from 75 - 3640 ppm (0.075-3.64 kg/m^3) in concrete [13].

Chapter 8

Numerical Results

Figure 8-1 shows the FEM model of control specimen. A large moisture movement was revealed in the control specimen without a CFRP layer by the numerical study of the water permeability.

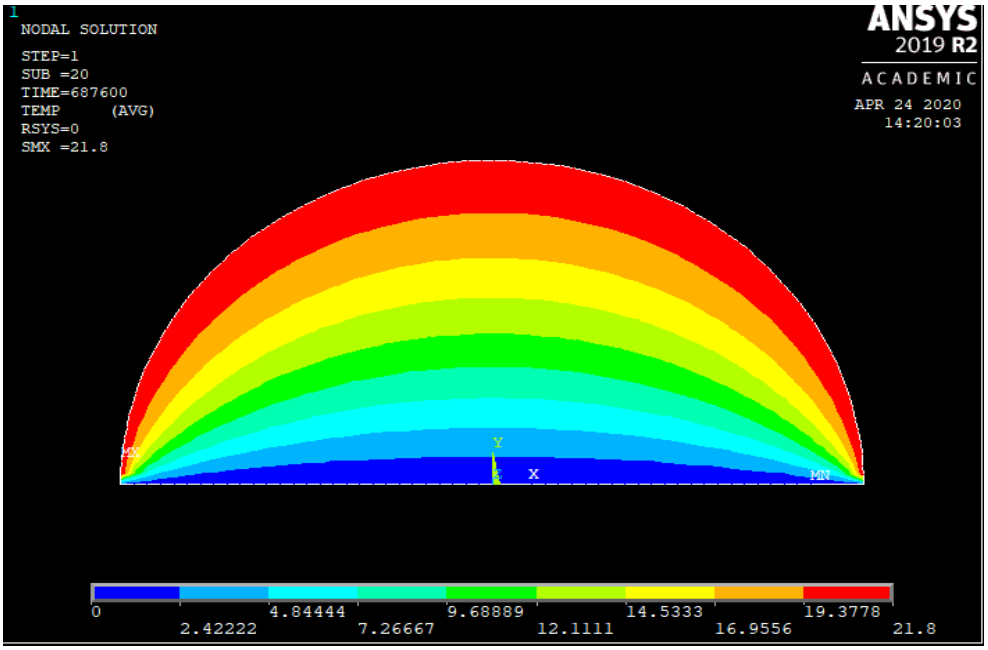

Figure 8-1- Control specimen without CFRP (water permeability)

Figures 8-2 and 8-3 show the numerical nodal solution of regular CFRP-wrapped normal & high strength concrete. It was observed from the numerical result of the water permeability that the moisture movement of the regular CFRP-wrapped normal strength and high strength concrete were within the zones of epoxy and concrete.

Figures 8-4 and 8-5 show the numerical nodal solution of presaturated CFRP. It was observed from the numerical result that the moisture movement in the high strength concrete wrapped with presaturated CFRP had lower diffusion than that of the presaturated CFRP-wrapped normal strength concrete.

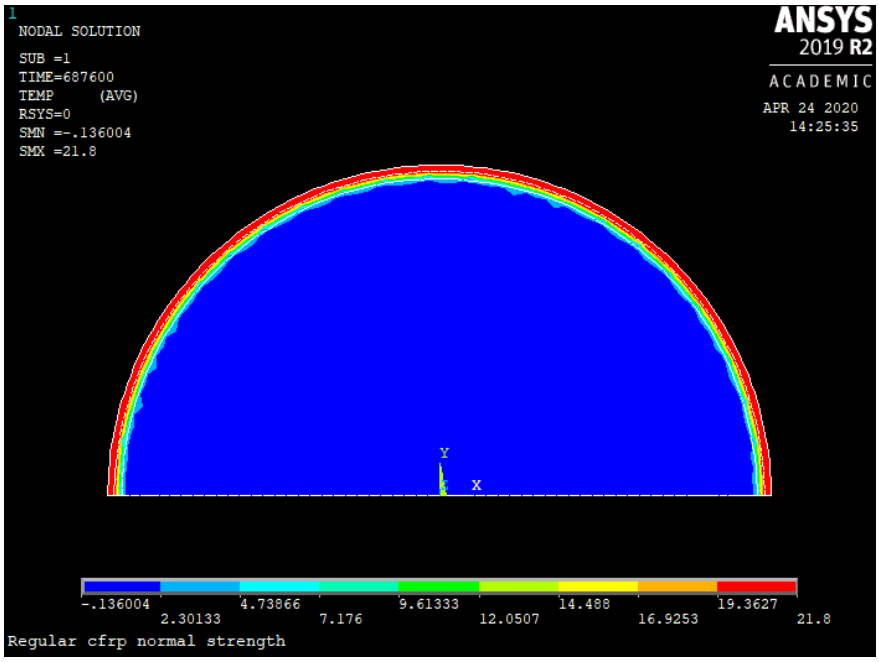

Figure 8-2 Regular CFRP normal strength concrete (water permeability)

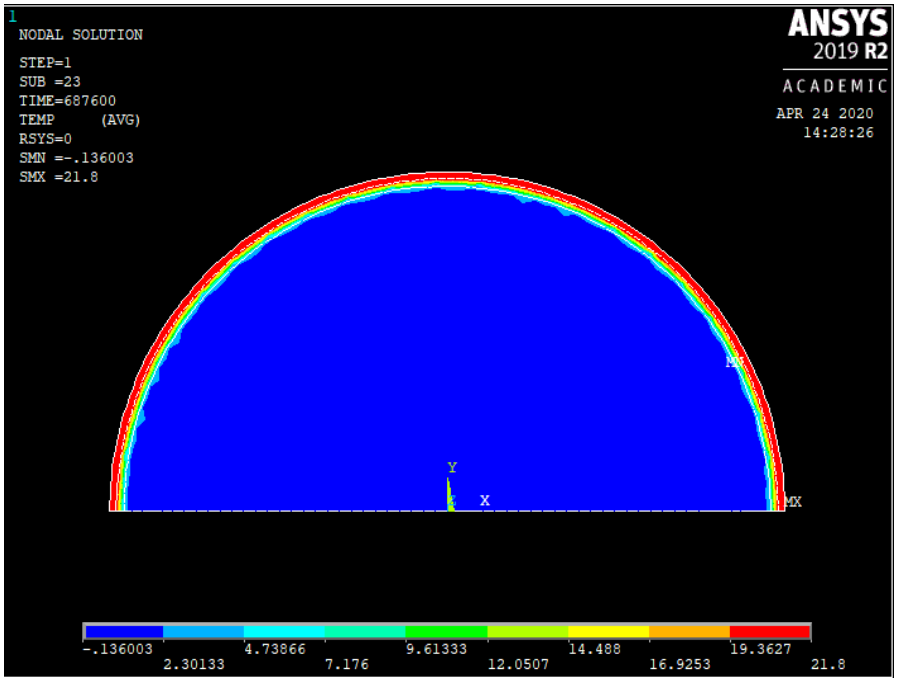

Figure 8-3 Regular CFRP high strength concrete (water permeability)

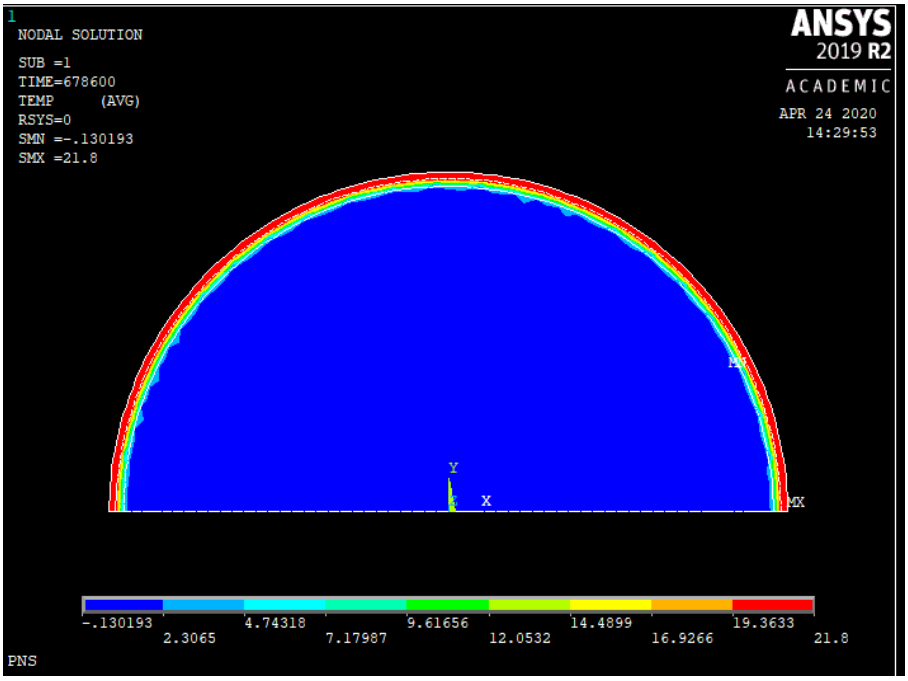

Figure 8-4 Presaturated CFRP normal strength concrete (water permeability)

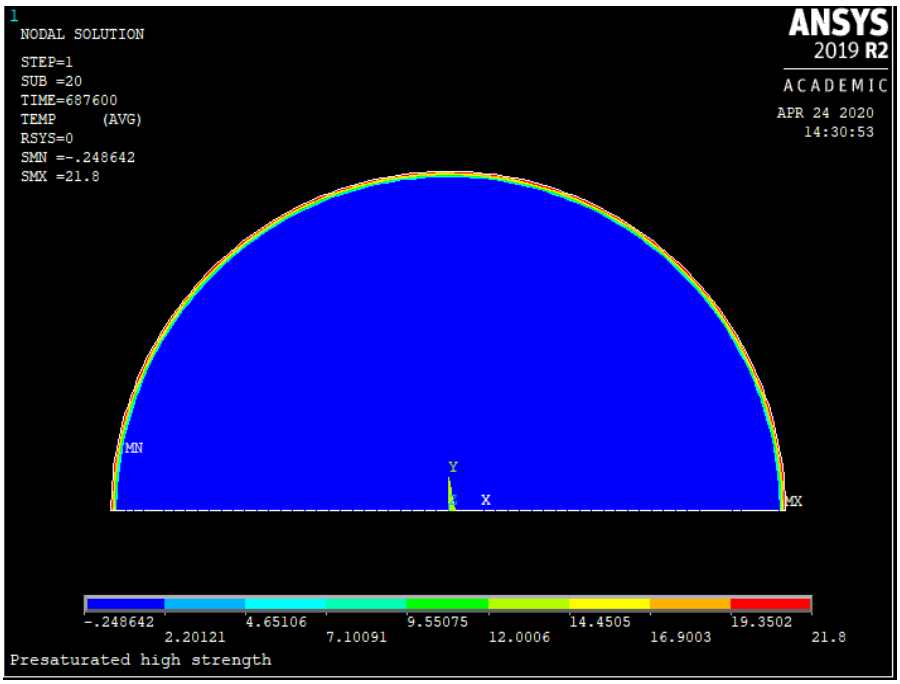

Figure 8-5 Presaturated CFRP high strength concrete (water permeability)

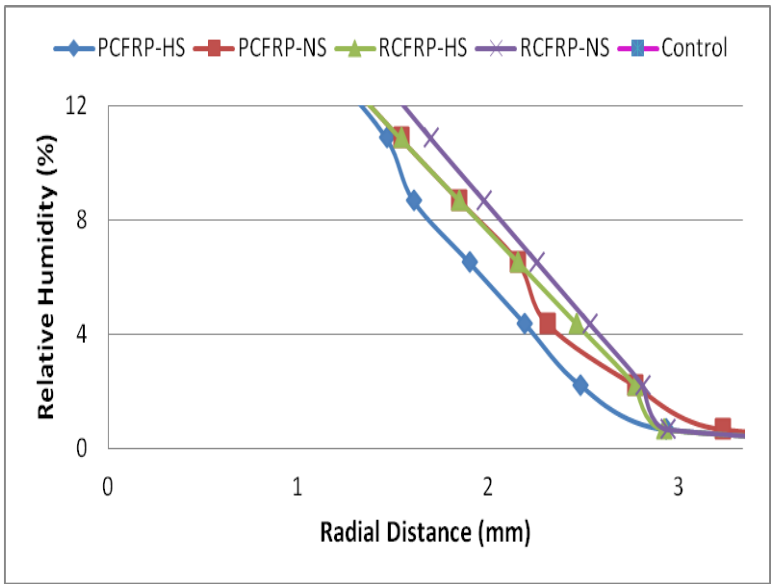

Figure 8-6 Water permeability partial plot of relative humidity vs radial distance

Figure 8-6 presents a comparison of the moisture movement for nine days in a control specimen without a CFRP layer, a regular CFRP, and a presaturated CFRP. The partial graph was plotted between the percent of relative humidity at 9 days and the depth (mm) and reveals that the relative humidity is expected to be higher in the control specimen without a CFRP layer. It also shows that the regular CFRP specimens with normal and high strength concrete and the presaturated CFRP specimens with normal strength concrete followed trends similar to those observed in the normal and high strength concrete with regular CFRP and the normal strength concrete with presaturated CFRP,as shown in Figure 8-6. It was observed from the experimental water absorption test results that the numerically predicted moisture content in the presaturated CFRP-wrapped high strength concrete was low and acted as an excellent barrier to corrosion.

Figure 8-7 shows the FEM model of the control specimen. It was observed from the numerical result that the chloride ingress and content in the unwrapped control model was higher than in the wrapped CFRP laminate.

Figures 8-8 and 8-9 show the numerical nodal solution of regular CFRP for both

normal & high strength concrete. It was observed that the chloride ingress and content of the regular CFRP-wrapped normal and high concrete models were within the zones of the epoxy and concrete.

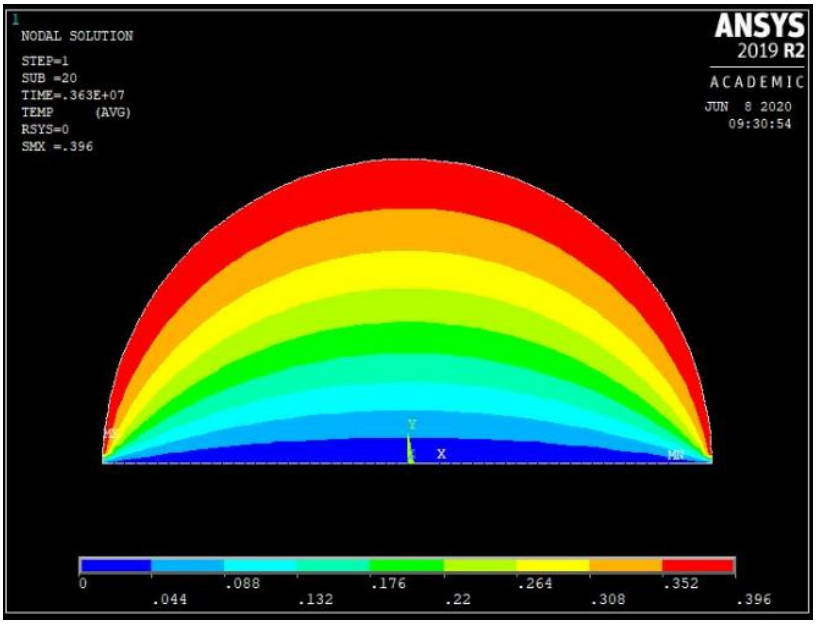

Figure 8-7 Control specimen without CFRP (chloride ingress)

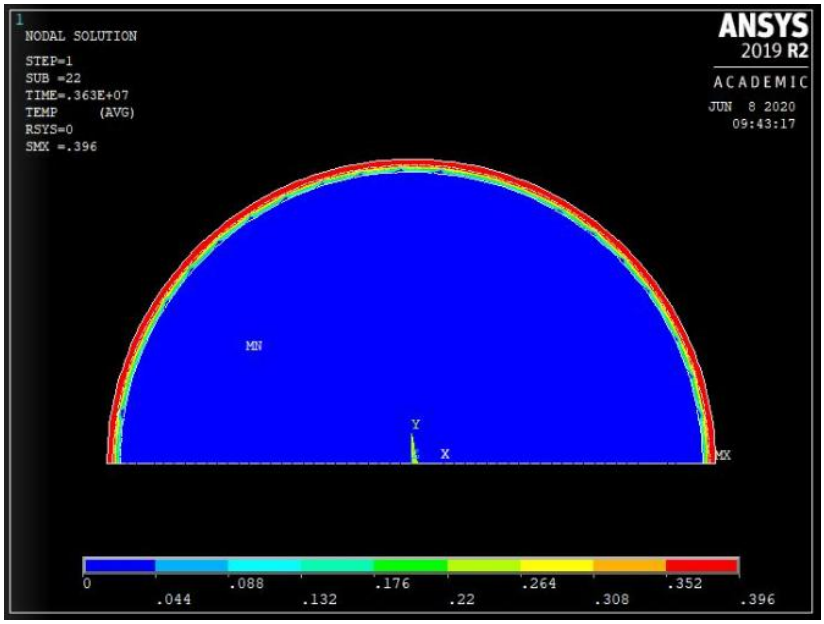

Figure 8-8 Regular CFRP normal strength concrete (chloride ingress)

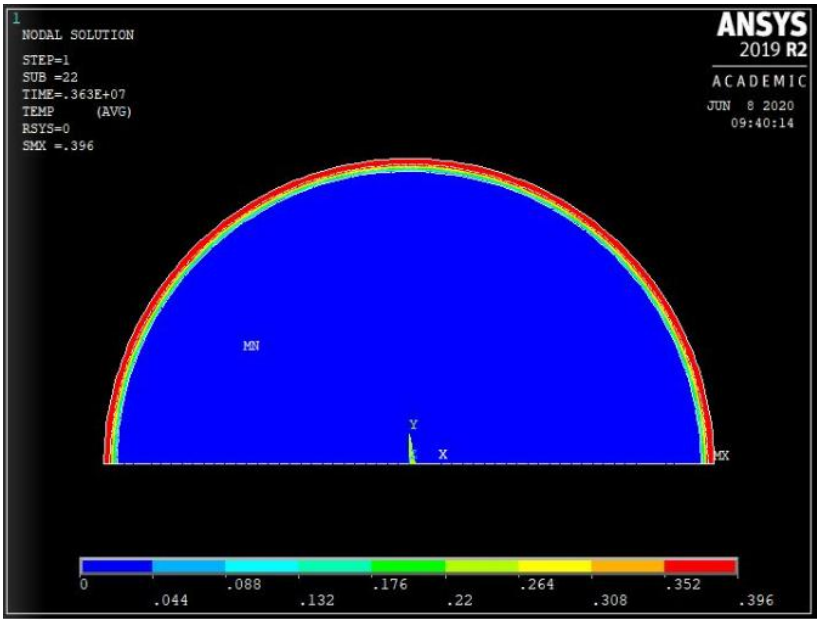

Figure 8-9 Regular CFRP high strength concrete (chloride ingress)

Figures 8-10 and 8-11 show the numerical nodal solution of presaturated CFRP. It was observed that the ingress of the chloride into the presaturated CFRP-wrapped high strength concrete specimen provided a more effective barrier to corrosion than it did in the presaturated CFRP-wrapped normal strength concrete

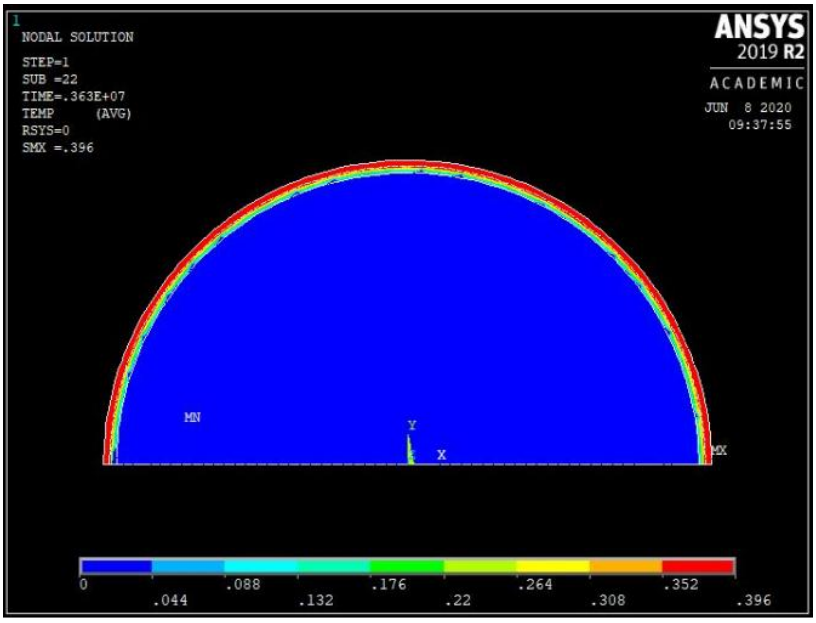

Figure 8-10 Presaturated CFRP normal strength (chloride ingress)

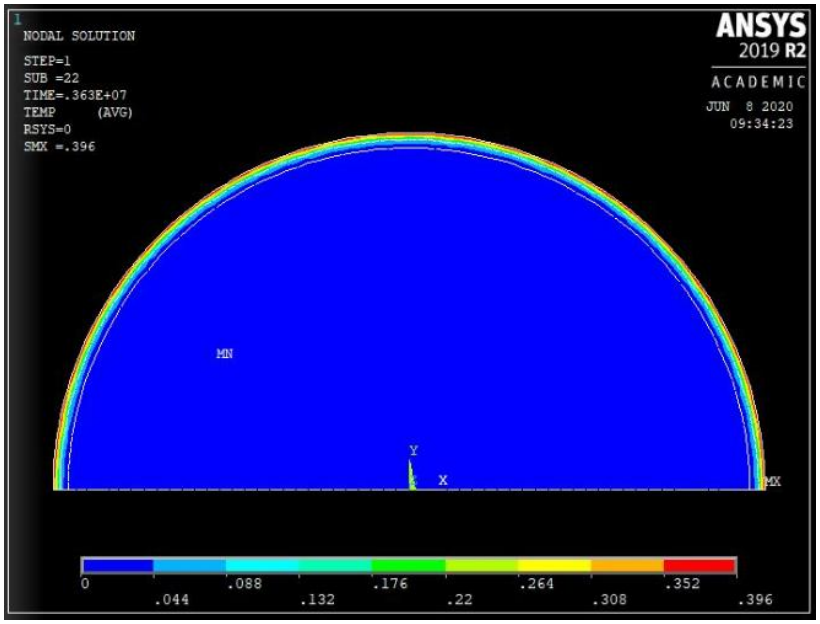

Figure 8-11 Presaturated CFRP high strength concrete (chloride ingress)

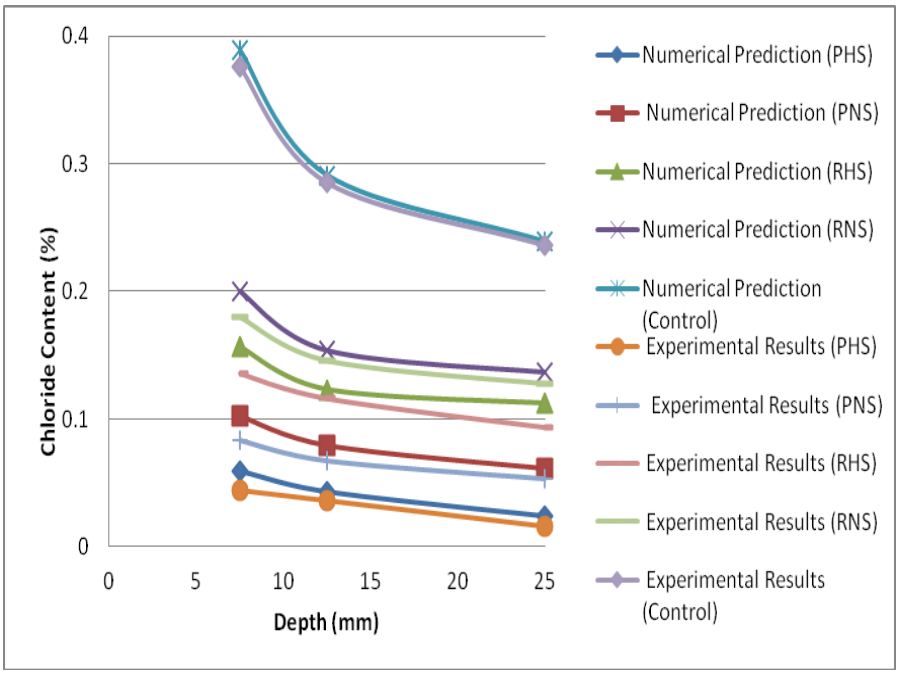

Figure 8-12 Graphical plot of chloride ingress: Experimental Results vs Numerical Prediction

Figure 8-12 compares the chloride content from the experiment with the numerical model prediction. As it can be observed, the results show a good agreement.

Figures 8-13 and 8-14 show the graph of time-dependent chloride ingress for a TxDOT without CFRP at 10 years, 25 years, 50 years, and 100 years. The graph shows that the chloride threshold limit was exceeded and the chloride content was expected to be higher than in the CFRP-wrapped column.

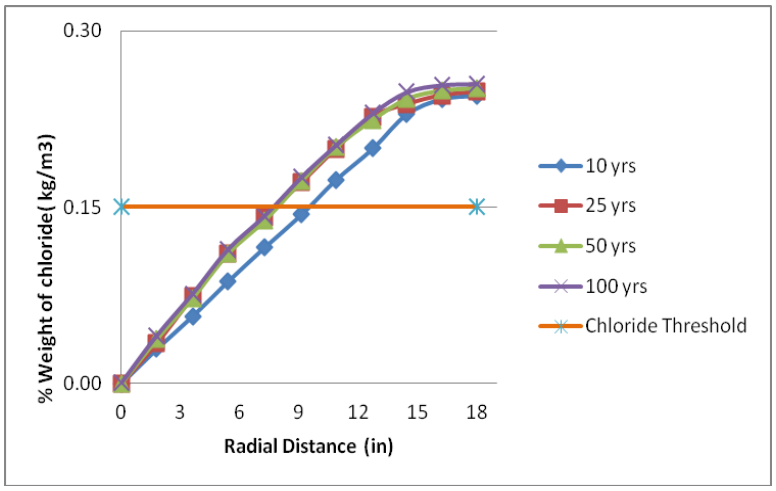

Figure 8-13 Time-dependent chloride ingress plot for control without CFRP

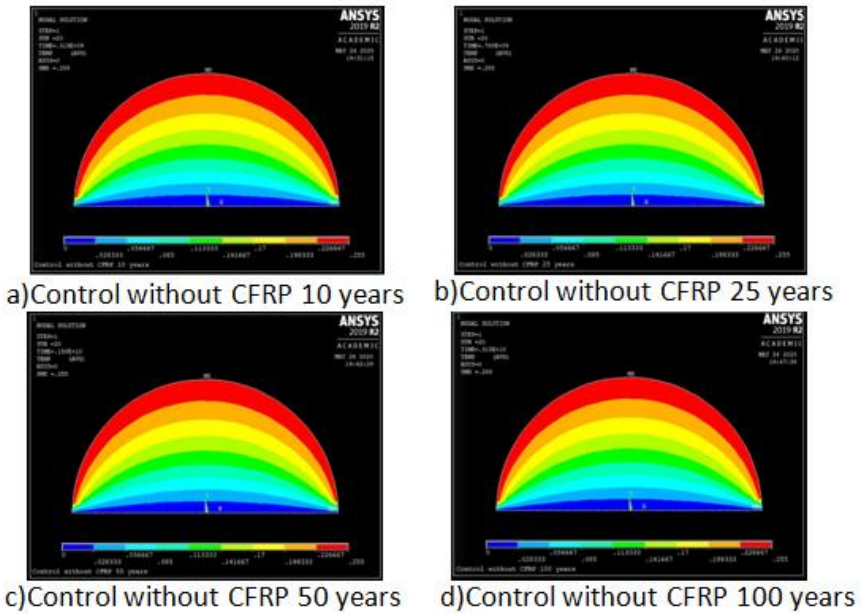

Figure 8-14 Time-dependent chloride ingress for control without CFRP

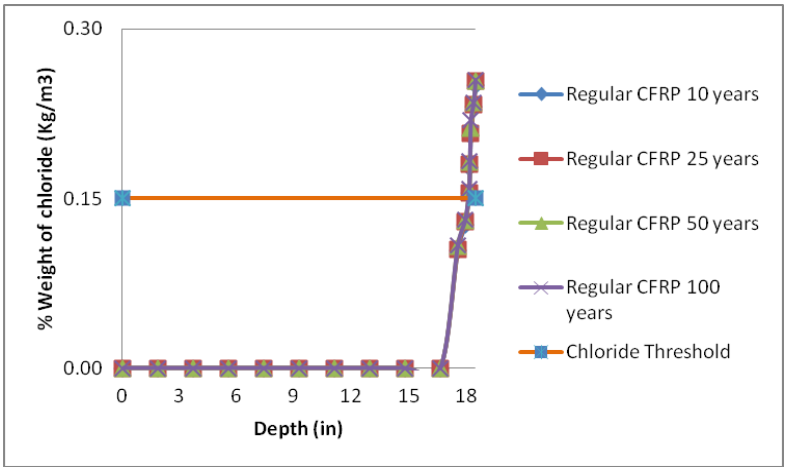

Figure 8-15 Time-dependent chloride ingress plot for regular CFRP

Figures 8-15 and 8-16 show the graph of time-dependent chloride ingress for a TxDOT column wrapped with regular CFRP at 10 years, 25 years, 50 years, and 100 years. The graph shows that the regular CFRP-wrapped column performed better than the control column without CFRP. The chloride content is expected to be lower in the regular CFRP-wrapped column than in the control column without CFRP. The chloride threshold limit value was reasonable.

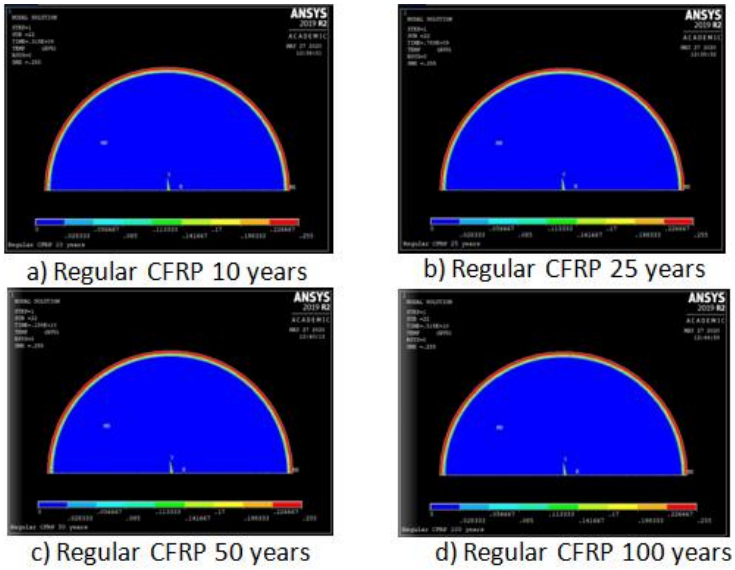

Figure 8-16 Time-dependent chloride ingress for regular CFRP

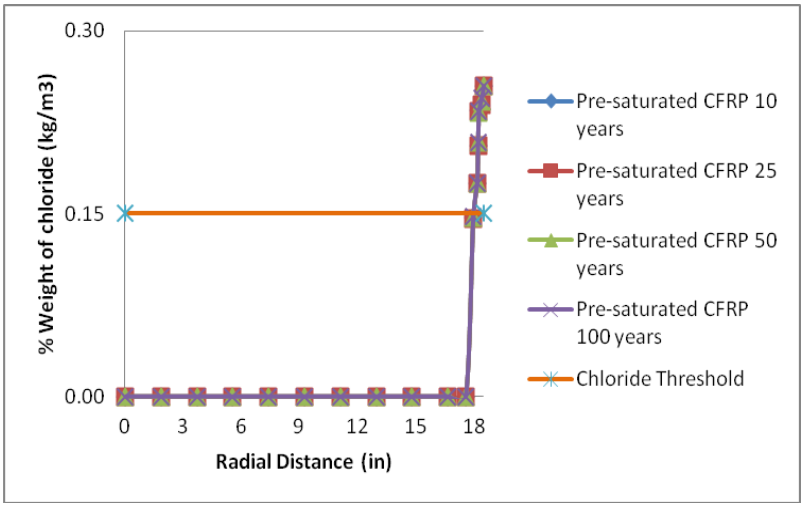

Figure 8-17 Time-dependent chloride ingress plot for presaturated CFRP

Figures 8-17 and 8-18 show the graph of time-dependent chloride ingress for a TxDOT column wrapped with presaturated CFRP at 10 years, 25 years, 50 years, and 100 years. The graph shows that the presaturated CFRP-wrapped column provided a stronger barrier to corrosion control than the regular CFRP. The chloride threshold limit value was low and did not exceed the 3" clear cover.

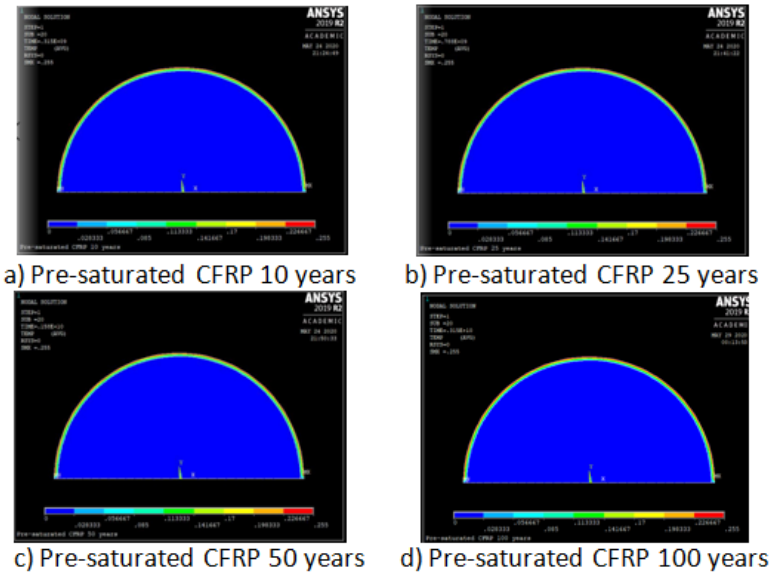

Figure 8-18 Time-dependent chloride ingress for presaturated CFRP

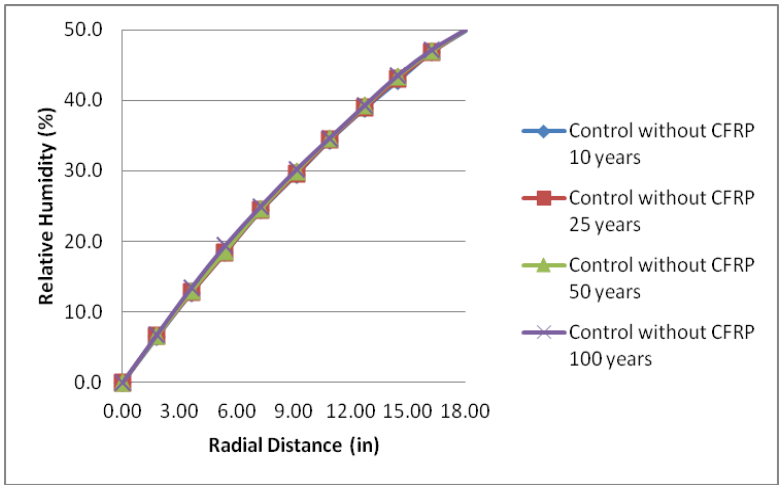

Figure 8-19 Time-dependent graph of control specimen without CFRP at 50% RH

Figures 8-19 and 8-20 show the graph of time-dependent water permeability for a TxDOT column without CFRP at 10 years, 25 years, 50 years, and 100 years. It was observed from the numerical analysis of the water permeability that the control specimen without a CFRP layer had a lot of moisture movement.

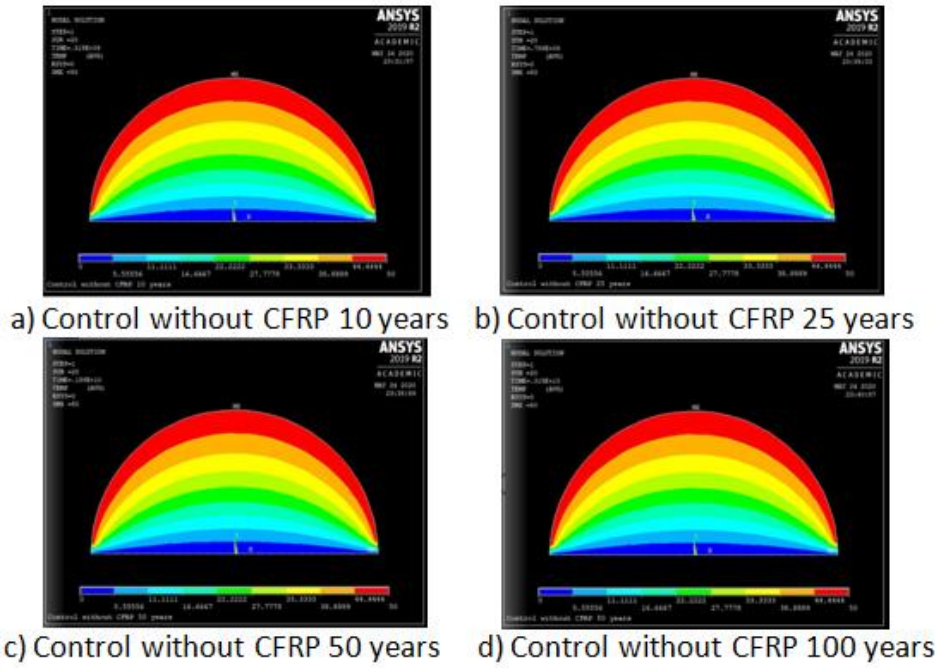

Figure 8-20 Time-dependent for control specimen without CFRP at 50% RH

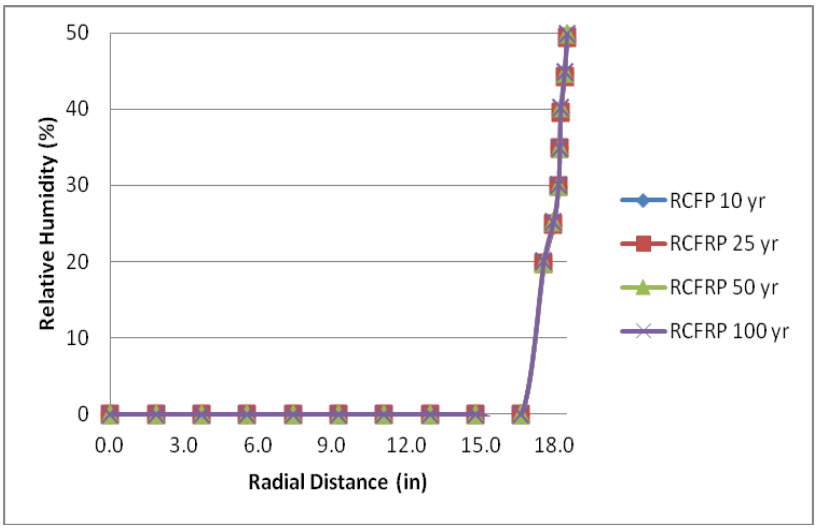

Figure 8-21 Time-dependent graph of regular CFRP-wrapped column at 50% RH

Figures 8-21 and 8-22 show the graph of time-dependent water permeability for a TxDOT column wrapped with regular CFRP at 10 years, 25 years, 50, years and 100 years. The graph shows that the moisture diffusion movement within the regular CFRP-wrapped column was within the zones of the epoxy and CFRP laminate.

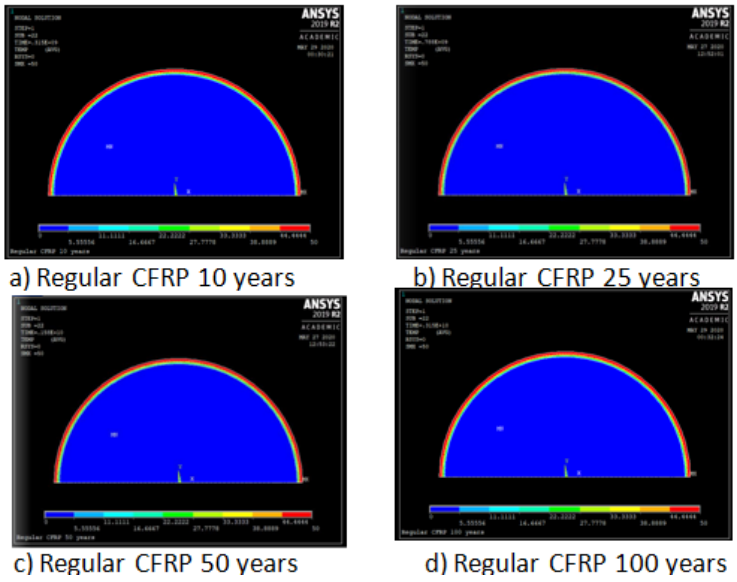

Figure 8-22 Time-dependent graph of regular CFRP-wrapped column at 50% RH

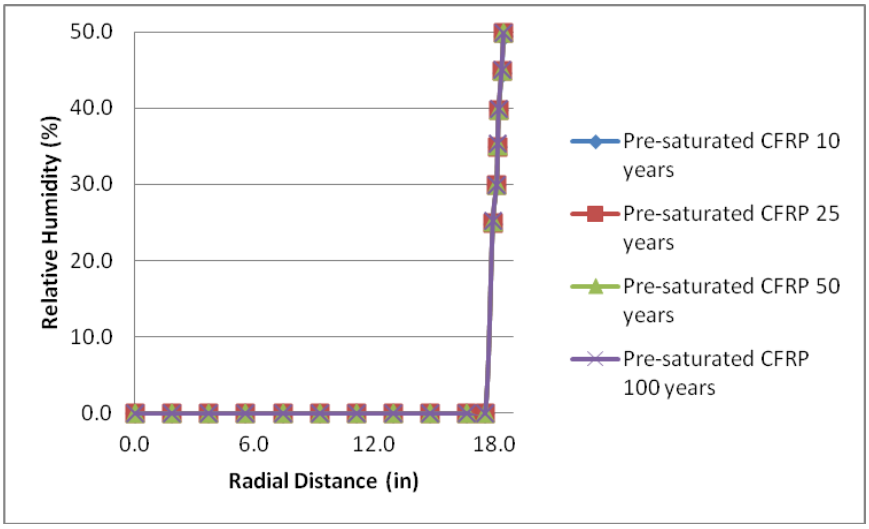

Figure 8-23 Time-dependent graph of presaturated CFRP-wrapped column at 50% RH

Figures 8-23 and 8-24 show a graph of time-dependent water permeability for a TxDOT column wrapped with presaturated CFRP at 10 years, 25 years, 50 years, and 100 years. The graph shows that the water movement in the presaturated CFRP-wrapped column was within the zone of the presaturated CFRP laminate and performed better against moisture diffusion than regular CFRP.

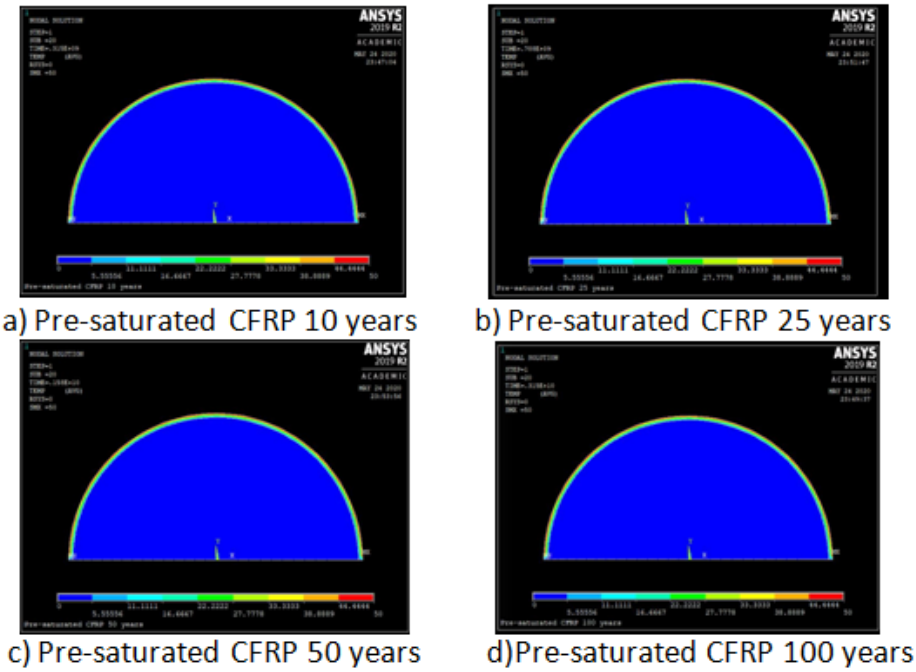

Figure 8-24 Time-dependent for presaturated CFRP-wrapped column at 50% RH

Chapter 9

Conclusions and recommendations

The significance of this study was to investigate whether presaturated CFRP applications reduce the ingress of water and chloride and increase the durability of concrete. The results described in Sections 5.1 and 5.2 indicate that presaturated CFRP applications reduce the ingress of water and provide a superior barrier to the ingress of sodium chloride. The following conclusions are based on the findings from this study.

1. An application of presaturated CFRP to concrete surfaces reduces the ingress of chloride and increases the concrete's durability. The chloride penetration percentage is lower than in normal strength and high strength concrete specimens without any application of CFRP. Most of the chloride is absorbed at the top of the concrete specimen and decreases with depth. The reduction of chloride in presaturated CFRP specimens varies between 0.016% at 25 mm, 0.036% at 12.5 mm, and 0.044% at 7.5 mm for high strength concrete specimens and 0.053 % at 25 mm, 0.067 % at 12.5 mm, and 0.083 % at 7.5 mm for normal strength concrete. For the regular CFRP-wrapped normal and high strength concrete specimens, the percent of reduction of the chloride ingress varies between 0.0128% and 0.093% at 25 mm. It may be concluded that a lower percent of chloride percentage reduces the corrosion rate and loss of load capacity. Presaturated CFRP applications can be used to extend the design life of a concrete structure.

2. This study is based on six weeks of chloride ingress data. Longer ponding periods would have resulted in greater chloride penetration, especially in the control samples without CFRP, and would have demonstrated more drastic differences between the specimens with and without CFRP, leading to larger reductions in the minimum clear covers.

3. Only one layer of CFRP was utilized in this study. Multiple layers of CFRP could result in a more dramatic reduction in the chloride ingress and absorption of water, as well as an increase in the concrete's durability and clear cover.

4. Presaturated CFRP wrapping on concrete surfaces decreases the amount of water that penetrates the concrete and increases its durability; the control specimens without CFRP absorb the most water varied between 3.64 mm and 2.5 mm with normal strength and high strength concrete specimens. The reduction of water permeability for presaturated CFRP applications varied between 0.3672 mm and 0.0408 mm with normal strength and high strength concrete specimens; however, the reduction of the water permeability for regular CFRP applications varied between 1.182 mm and 0.612 mm in normal strength and high strength concrete specimens. Therefore, it may be concluded that decreased water permeability reduces the corrosion rate and loss of load capacity.

5. The parametric study showed that the long-term durability of TxDOT columns varied, depending on the type of CFRP, the thickness of the CFRP, and the tensile modulus of the CFRP. The current study suggests that CFRP-wrapped columns reduce the clear cover to 1.5".

Future research is recommended, based on the findings of this study, as follows:

1. The use of multiple layers of wrapped CFRP laminates on concrete should be explored to obtain the equivalent clear cover depths for a longer period of sodium chloride exposure. It is recommended that the concrete be exposed to the chemical reagent for a period of at least 12 months.

2. The effects of exposing concrete with CFRP wrapping to other corrosion-causing agents, such as chemicals and elevated temperatures should be investigated.

Appendix –A

Modeling of 2 D Column (Water Permeability)

- Main Menu/preprocessor/material properties/material library/selectunits
- Main Menu/Preprocessor/Thermal/h-Method
- Main Menu/Preprocessor/Element Type/add/edit/delete/solid/PLANE77
- Main Menu/ Preprocessor/Material Properties/Material Models/Thermal/Conductivity/Isotropic/KXX
    - ❖ Set different conductivities with temperature, as presented in Table 4.1.
    - ❖ Name this model as concrete.
- Material/New Model/Thermal/Conductivity/Isotropic-KXX
    - ❖ Set different conductivities with temperature, as presented in Table 4.1.
    - ❖ Name this model as epoxy and repeat same for regular CFRP and presaturated CFRP.
- Main Menu/Preprocessor-/Material Properties/Material Models/ Density
    - ❖ Set density for concrete, epoxy, and FRP for temperature.
- Main Menu/Preprocessor-/Material Properties/Material Models/ Specific Heat
    - ❖ Set specific heat for concrete, epoxy, and FRP for temperature.
- Main Menu/Preprocessor/Modeling/Create/Areas/Circle/ By Dimensions/ Outer radius (52.2), Inner radius (51.2) and angle 0^0 to 180^0
- Main Menu/Preprocessor/Modeling/Create/Areas/Circle/By Dimensions / Outer radius (51.2) and Inner radius (50) and angle 0^0 to 180^0
- Main Menu/Preprocessor/Modeling/Create/Areas/Circle /By Dimensions / Outer radius (50) and Inner radius (0) and angle 0^0 to 180^0
- Main Menu/Preprocessor/Operate Meshing/Mesh Attributes/Picked Areas/ Material #1 or Material#2 or Material#3

- Main Menu/Preprocessor/Meshing/Size Controls/ Manual Size/Global/Size/0.5
- Main Menu/Preprocessor/Modeling/Operate/Boolean/Glue/Area/Pick All/Ok
- Main Menu/Preprocessor/Meshing/Mesh/Areas/Free/Pick All/Ok
- Utility Menu/Plot Controls/ Numbering/Material Numbers/Ok
- Main Menu/Solution/Define Loads/Apply/Thermal/Convections on Lines-film coefficient bulk temperature
    - ❖ Set Film coefficient to 0 for all of the bottom lines.
- Solution/ Analysis Type/ New Analysis/ Transient/Full
- Solution/ Analysis Type/ Sol'n Control/
    - ❖ Set time and automatic time steeping; set the number of sub steps to 20, maximum number of sub-steps to 100, and minimum number of sub-steps to 20.
    - ❖ Set the frequency to write every sub step.
    - ❖ Set the line search on.
    - ❖ Set the maximum number of iterations to 100.
- Main Menu/Solution/define Loads/ Apply/Initial condition/ Define/
    - ❖ Select the concrete area and set to 30.
    - ❖ Select the FRP and epoxy area and set to 0.
- Main Menu/Solution/define Loads/ Apply/Thermal/ Temperature/On Lines
    - ❖ Set all lines to 21.8
- Utility Menu/Plot Controls/Symbols/Show Press and Count as Arrows/Ok
- Main Menu/Solution/Solve/Current LS/Ok
- General Post proc/Plot Results/Contour Plots/Nodal Solution/ DOF solution
- Utility menu/Plot Ctrls/Animate/Over Time

Modeling of 2 D Column (chloride Ingress)

- Main Menu/preprocessor/Material properties/material Library/Select/Units
- Main Menu/Preprocessor/Thermal/h-Method
- Main Menu/Preprocessor/Element Type/add/edit/delete/solid/PLANE55
- Main Menu/ Preprocessor/Material Properties/Material Models/Thermal/Conductivity/Isotropic/KXX
    - ❖ Set different conductivities with temperature as presented in Table 4.1.
    - ❖ Name this model as concrete.
- Material/New Model/Thermal/Conductivity/Isotropic-KXX
    - ❖ Set different conductivities with temperature as presented in Table 4.1.
    - ❖ Name this model as epoxy and repeat same for regular CFRP and presaturated CFRP.
- Main Menu/Preprocessor-/Material Properties/Material Models/ Density
    - ❖ Set density for concrete, epoxy, and FRP for temperature.
- Main Menu/Preprocessor-/Material Properties/Material Models/ Specific Heat
    - ❖ Set specific heat for concrete, epoxy, and FRP for temperature.
- Main Menu/Preprocessor/Modeling/Create/Areas/Circle/ By Dimensions/ Outer radius (52.2), Inner radius (51.2) and angle 0^0 to 180^0
- Main Menu/Preprocessor/Modeling/Create/Areas/Circle/By Dimensions / Outer radius (51.2) and Inner radius (50) and angle 0^0 to 180^0
- Main Menu/Preprocessor/Modeling/Create/Areas/Circle /By Dimensions / Outer radius (50) and Inner radius (0) and angle 0^0 to 180^0
- Main Menu/Preprocessor/Meshing/Size Controls/ Manual Size/Global/Size/0.5
- Main Menu/Preprocessor/Meshing/Mesh/Areas/Free/Pick All/Ok

- Utility Menu/Plot Controls/ Numbering/Material Numbers/Ok
- Main Menu/Solution/Define Loads/Apply/Thermal/Convections on Lines-film coefficient bulk temperature

    - ❖ Set film coefficient to 0 for all the bottom lines.

- Solution/ Analysis Type/ New Analysis/ Transient/Full
- Solution/ Analysis Type/ Sol'n Control/

    - ❖ Set time and automatic time steeping; set the number of sub steps to 20, maximum number of sub-steps to 100, and minimum number of sub-steps to 20.
    - ❖ Set frequency to write every sub step.
    - ❖ Set line search on.
    - ❖ Set maximum number of iterations to 100.

- Main Menu/Solution/define Loads/ Apply/Initial condition/ Define/
    - ❖ Define initial condition/temperature/ 0.
- Main Menu/Solution/define Loads/ Apply/Thermal/ Temperature/On Lines
    - ❖ Set all lines to 7.06.
    - ❖ Do not set temperature on left lines because this is center of the model.

- Utility Menu/Plot Controls/Symbols/Show Press and Count as Arrows/Ok
- Main Menu/Solution/Solve/Current LS/Ok

- General Post proc/Plot Results/Contour Plots/Nodal Solution/ DOF solution
- Utility menu/Plot Ctrls/Animate/Over Time

Appendix –B

ASTM C1152-12 Example calculation

Using equation from ASTM 1152, percentage of chloride ingress is calculated for

$$CL\% = 3.45\left[\left(\frac{V_1 - V_2}{W}\right)N\right] \qquad (1)$$

Where,

V_1 = mL of 0.05 N AgNO solution used for sample titration (equivalence point) V_2 = mL of 0.05 N AgNO solution used for blank titration (equivalence point) N = normality of the 0.05 N $AgNO_3$ solution & W = mass of sample in (g)

For control specimen normal strength concrete at 7.5 mm,

W = 10.36 g

V1 = 23.2 ml

V2 = 0 (Blank titration)

$$CL\ \% = 3.45\left[\frac{(23.2 - 0)0.05}{10.36}\right] = 0.397\ \%$$

Appendix –C

ASTM C1585-13 Example calculation

$$Rate\ of\ absorption, I = \frac{m_t}{a * d}$$

Where,

I = the absorption,

m_t = the change in specimen mass in grams, at the time t,

a = the exposed area of the specimen, in mm^2, and

d = the density of the water in g/mm^3

$$I = \frac{0.62}{8107 * 0.0010} \qquad = 0.0764\ mm$$

Appendix D

Diffusion coefficient calculation (Ryan J.M)

$$Diffusion\ Coefficient\ (D) = 3.14\left(\frac{h}{4 * Mmax}\right)^2\left[\left(\frac{M2 - M1}{\sqrt{t2 - t1}}\right)^2\right]$$

Where,

M1 and M2, are the weight percentage moisture (wt %) taken at times t1 and t2 (in seconds)

h is the laminate thickness, in mm and

Mmax is the equilibrium moisture level (wt %) for the given RH.

$$Diffusion\ Coefficient\ (D) = 3.14\left(\frac{1}{4 * 3.16}\right)^2\left[\left(\frac{9.66}{\sqrt{829}}\right)^2\right] = 4.26973\ X\ 10^{-5}\ mm/s$$

Appendix –E

TOOLS USED FOR INSTALLATION

The table below contains tools that are commonly required for the application of FRP wrap on concrete specimens described in Section 1.

Table A.1 Tools used for installing the various products

No.	Tool	Purpose
1	Disk Grinder	Leveling out imperfections on the concrete surface
2	Power Washer, Soft Brush & Putty Knife	Cleaning concrete surface
3	Mixing Containers	Measuring and blending of the two-part epoxy system
4	Weight Scale (A)	Weighing of the main agent and hardener
5	Hand-held Mixer with Paddle Blade	Mixing the two epoxy components
6	Putty Knife (A)	Mixing and applying putty

7	Disposable Brush or Rollers	Applying epoxy
8	Scissors	Cutting fiber sheets
9	Fiberglass Compaction Steel Roller	Evenly spreading out epoxy into glass fiber
10	Temporary Trough	Workstation for saturating glass fibers with epoxy
11	Paddle Wheel	Promotes epoxy impregnation by removing air between the fiber sheet and the concrete surface
12	Dust Masks	Prevent inhalation of fumes and dust
13	Goggles & Gloves	Prevent epoxy system from touching skin and eyes
14	Acetone	Clean-up product for tools

References

1. ACI Committee 440 (2017). Guide for the Design and Construction of Externally Bonded FRP Systems for Strengthening Concrete Structures. (ACI 440.2R-17), American Concrete Institute, Farmington Hills, Michigan, USA.
2. American Society of Civil Engineers (ASCE). Report Card for America's Infrastructure. ASCE, 2017.
3. American Society for Testing and Materials (ASTM). (2012). Standard Test method for Acid-soluble Chloride in Mortar and Concrete. ASTM C1152-12.
4. American Society for Testing and Materials (ASTM). (2015). Standard Test Method for Chemical Analysis of Hydraulic Cement. ASTM C114-15.
5. American Society for Testing and Materials (ASTM). (2013). Standard Test Method for Measurement of Rate of Absorption of Water by Hydraulic-Cement Concretes. ASTM C1585 - 2013.
6. Anil, O., & Belgin, C. M. (2010). "Anchorages Effects on CFRP-to-Concrete Bond Strength". *Journal of Reinforced Plastics and Composites*, 29(4), 539–557.
7. Ashour et al (2018). "Analytical and Experimental Study on Upgrading the Seismic Performance of Reinforced Masonry Columns Using GFRP and CFRP Wraps." American Society of Civil Engineers, *Journal of Composites for Construction*, ASCE, ISSN 1090-0268.
8. Chuanqing Fu et al (2010). "Modeling of Chloride Ions Diffusion in Cracked Concrete," *Earth and Space 2010: Engineering, Science, Construction and Operations in Challenging Environments.* ASCE pp.3579-3589.
9. Conciatori et al. (2008). "Capillary Suction and Diffusion Model for Chloride Ingress into Concrete". *Cem. Concr. Res.* 38, 1401–1408. doi:10.1016/j.cemconres.2008.06.006
10. Danny Wells et al (2014). "Sealants, Treatments and Deicing Salt Practices to Limit Bridge Deck Corrosion and Experimental Deck Sealants and Pier Cap Coating on Interstate 47." *Kentucky Transportation Center College of Engineering*. DOI: http://dx.doi.org/10.13023/KTC.RR.2014.04
11. ElSafty, A., Graeff, M. K., & Fallaha, S. (2014). "Behavior of Laterally Damaged Prestressed Concrete Bridge Girders Repaired with CFRP Laminates Under Static and Fatigue Loading." *International Journal of Concrete Structures* and *Materials*, *8*(1), 43–59. https://doi.org/10.1007/s40069-013-0053-0
12. Glass, G.K., and Buenfeld, N.R. "The Presentation of the Chloride Threshold Level for Corrosion

of Steel in Concrete." *Corrosion Science*, Vol. 39, No. 5, 1997, pp. 1001-1013.

13. Güneyisi et al.(2009). "Estimation of Chloride Permeability of Concretes by Empirical Modeling: Considering Effects of Cement Type, Curing Condition and Age." *Journal of Construction and Building Materials*, 23, 469–481.
14. Kobayashi , K., Kanakubo, T., & Jinno, Y. (2004). "Seismic Retrofit of Structures Using Carbon Fibers." *VIII Simposio Nacional De Ingenieria Sismica*, pp. 1-21.
15. Kaushik, S.K., and Islam, S. "Suitability of Sea Water for Mixing Structural Concrete Exposed to a Marine Environment. *Cement & Concrete Composites*, 1995. 17: p. 177-185.
16. Malvar, L . J., Warren, G. E and Inaba, C. (1995). "Rehabilitation of Navy Pier Beams with Composite Sheets." *Non-Metallic (FRP) Reinforcement for Concrete Structures; Proceedings of the 2nd International RILEM Symposium,* London, England, pp. 534-540.
17. Mahmoud et.al, (2015). "Multi-scale Response of Sustainable Self-Compacting Concrete (SCC) to Carbonation and Chloride Penetration."
18. Mohsen A. Issa and Atef Khalil (2010). "Diffusivity and Permeability of High Performance Concrete for Bridge Decks." *PCI Journal,* Spring 2010.
19. Orton, S. L. Jirsa, J.O et.al. (2008). " Design Considerations of Carbon Fiber Anchors." *Journal of Composites for Construction,* Vol. 12, No. 6, pp. 608-616.
20. Ouyang, Z. and Wan, B. (2008), " Modeling of Moisture Diffusion in FRP Strengthened Concrete Specimens." *Journal of Composites for Construction,* ASCE, Vol.12 No.4,pp. 425-434.
21. Rafaat and Mark. (2010). "Effect of Severe Environmental Exposures on Wrapped Concrete Columns CFRP." *Journal of Composites for Construction* © ASCE/ January/February 2010.pp. 83-93.
22. Reddy D.V et al (2006). "Cost-Effective Repairs of Marine Corrosion Damage." *Fourth LACCEI International Latin American and Caribbean Conference for Engineering and Technology (LACCET'2006)* "Breaking Frontiers and Barriers in Engineering: Education, Research and Practice" 21-23 June 2006, Mayagüez, Puerto Rico.

1. Ryan J.M (2009) PhD Dissertation, Materials Research Centre, School of Engineering, Swansea University.
2. Sangeeta et al (2009). "Corrosion of Steel Reinforcements Embedded in FRP Wrapped Concrete." *Construction, Buildings and Materials*, 23(1), 153–161.
3. Stephen R. Sharp (2016). "Use of Electrochemical Chloride Extraction and Associated Repairs to Extend the Beneficial Life of Reinforced Concrete Substructures." Virginia Transportation Research Council (A partnership of the Virginia Department of Transportation and the University of Virginia).
4. Syed Ishtiaq Ahmad and Mohammad Anwar Hossain (2017). "Water Permeability Characteristics of Normal Strength Concrete Made from Crushed Clay Bricks as Coarse Aggregate." *Hindawi Advances in Materials Science and Engineering.* Vol. 2017.

5. Triantafillou, T. C. (1998). “Shear Strengthening of Reinforced Concrete Beams Using Epoxy bonded FRP Composites.” *ACI Structural Journal,* Vol. 95, No. 2, pp. 107-115.
6. Texas Department of Transportation (2018). Bridge Detailing Guide.
7. Weitsman, Y. (1977) “Stresses in Adhesive Joints Due to Moisture and Temperature.” *Journal of Composites Materials*, pp.378–394.
8. Wittmann (2009). “Influence of Surface Impregnation with Silane on Penetration of Chloride into Cracked Concrete and on Corrosion of Steel Reinforcement.” *International Journal of Modeling Identification and Control*, Vol.7, No.2, pp.135-141.
9. Yazdani and Gracia (2014). “Effect of Fiber Reinforced Polymer Wrapping on Concrete Chloride Penetration and Concrete Cover.” *Journal of the Transportation Research Board, Washington*, pp. 98-104.
10. Yazdani and Goucher (2015). “Increasing Durability of Light Weight Concrete through FRP Wrap.” *Elsevier Composites Part B: Engineering* Volume 82, 1 December 2015, Pages 166-172.
11. Yazdani et al (2017). “Effect of FRP Wrapping on Concrete Chloride Ingress.” *International Journal of Current Research*, Vol.9 Issue, 01, pp.44623-44629.
12. Yungon Kim (2012). “Shear Strengthening of Reinforced and Prestressed Concrete Beams Using Carbon Fiber Reinforced Polymer (CFRP) Sheets and Anchors.” Centre for Transportation Research, The University of Texas, Austin. TxDOT Project Number 0-6306.

Bibliographical Information

Ramya Anandhan earned her master's degree in structural Engineering at Vellore Institute of Technology, India in 2016. She received her bachelor's degree in civil engineering from Anna University, India in 2011. She worked as lecturer in the Department of Civil Engineering at Magna College of Engineering from 2011-2013. Later she worked as a design engineer at Spark Consulting Private Limited where she got hands-on experience that includes shed, scaffolding, elevation, interior, demolition, new building, and e-permitting for a New York City project. She plans to get her PE license and continue learning and gaining professional experience in the work force.